Fall 2015

Design of an Attitude Control System for Spin-Axis Control of a 3U CubeSat

Alexander Joseph Westfall
San Jose State University

DESIGN OF AN ATTITUDE CONTROL SYSTEM FOR SPIN-AXIS CONTROL OF A 3U CUBESAT

A Thesis

Presented to

The Faculty of the Department of Aerospace Engineering

San José State University

In Partial Fulfillment

of the Requirements for the Degree

Master of Science

by

Alexander J. Westfall

December 2015

The Designated Thesis Committee Approves the Thesis Titled

DESIGN OF AN ATTITUDE CONTROL SYSTEM FOR SPIN-AXIS CONTROL OF A 3U CUBESAT

by

Alexander J. Westfall

APPROVED FOR THE DEPARTMENT OF AEROSPACE ENGINEERING

SAN JOSÉ STATE UNIVERSITY

DECEMBER 2015

Dr. Periklis Papadopoulos	Department of Aerospace Engineering
Dr. Sean Swei	Department of Aerospace Engineering
Dr. Marcus Murbach	Department of Aerospace Engineering

ABSTRACT

DESIGN OF AN ATTITUDE CONTROL SYSTEM FOR SPIN-AXIS CONTROL OF A 3U CUBESAT

by Alexander J. Westfall

This paper describes the design process of developing a spin-axis control system for a 3U CubeSat, a relatively small satellite. Design requires the CubeSat to de-spin after deployment and direct its antenna to track Earth nadir position. The one degree of freedom controller is developed for the TechEdSat, which is a CubeSat with a payload that allows for the assumption that rotation pitch and yaw rates are sufficiently close to zero. Satellite torqueing disturbances are modeled with reaction wheel noise for a more complete system analysis. Sensor noise is unmodeled. Frequency domain and time domain analyses are presented; the entire system bandwidth operates at 0.08 hertz with 43.2 decibels of gain and 67.7^{o} of phase margin. During nominal operations, pointing accuracy with perfect state knowledge assumption maintains position with steady state error of 13.7 arc seconds and oscillates by 16.7 arc seconds at a rate of 0.7 mHertz. Artificial wheel noise is injected into the model causing the pointing accuracy to drop to ± 15 arc seconds. Environmental disturbances are modeled extensively; the magnetic field torque is the worst disturbance, at 4.2e-7 Newton-meters. A 0.2 Amp·m^2 magnetorquer dumps the excess momentum every 7.75 hours and require 1.5 hours to complete. In the deployment simulation, a 1 rotation per minute spin is arrested with no angular offset in 60 seconds. Future plans include utilizing the model to build and fly a prototype reaction wheel on a future TechEdSat mission to verify modeled expectations.

Acknowledgments

The author would like to thank the HelioCube Team for their efforts in the early design stages of this thesis. A hearty thank you also goes out to Professor Papadopoulos, whose connections and advisement lead to work on this project. Thank you as well to Dr. Sean Swei. I could not have hoped to accomplish what I have in the time I did without our many hours of meetings and discussions; your guidance and support has been essential to the success of this work. Another thank you must go out to Dr. Marcus Murbach, whose enthusiasm and willingness to provide information about the TechEdSat has given this project the perfect platform to develop a unique control system around.

Thank you to my wonderfully dedicated editor and partner, Erika Schmidt, who's longtime support gave me the courage and strength to begin (and finish) my master's degree.

Table of Contents

List of Tables

List of Figures

Nomenclature

A, a = Variables

$\dot{A}$ = Time derivative of variable

$\hat{A}$ = Area, m^2

A_s = Area of spacecraft in direction of orbital velocity, m^2

$\boldsymbol{B}$ = Magnetic field vector, Tesla

B_e = Earth's magnetic dipole strength, Tesla

b = Viscous friction, N·m·sec

BEMF = Back Electro Magnetic Force, N·m

C_d = Coefficient of drag

C_m = Center of mass, m

C_p = Center of pressure, m

c = Speed of light, m/sec

ECIF = Earth Centered Inertial Frame

$\boldsymbol{H}$ = Angular momentum vector, N·m/sec

$\boldsymbol{I}$ = Inertia matrix, $kg \cdot m^2$

K = Control gain

K_d = Derivative control gain

K_{mag} = Magnetic control gain

K_v = Back EMF voltage transformation gain

M = Moment, N·m

m = Mass, kg

$\boldsymbol{P}$ = A point located in inertial space

$[\boldsymbol{Q}]_{Aa}$ = Transformation matrix from A to a

$\boldsymbol{q}$ = Quaternion vector

q_{rf} = Reflectance factor

$\boldsymbol{R}, \boldsymbol{r}$ = Position, m

R_m = Resistance of Motor, ohm

s = Laplace transformed domain space

T = Torque, N·m

t = Time, sec

$\boldsymbol{s_{cp}}$ = Distance vector from center of mass to center of pressure, m

$\widehat{\boldsymbol{u}_{\boldsymbol{e}}}$ = Nadir direction unit vector

$\widehat{\boldsymbol{u}_{\boldsymbol{V}}}$ = **U**nit vector in direction of travel

V = Velocity, m/s

ΔA = Change in variable

δ = Perturbation

μ = Standard gravitational parameter of Earth, km^3/s^2

η_B, ξ_B, λ = Geomagnetic orbital parameters, degrees

ρ = Atmospheric density, kg/m^3

φ = Precession angle, degrees

θ = Nutation angle, degrees

$\widetilde{\theta_R}$ = True anomaly, degrees

θ_S = Solar incidence angle, degrees

τ_R = Orbital frequency, sec^{-1}

$\boldsymbol{\omega}$ = Rotational velocity, degrees/sec

ω_0 = Natural frequency, degrees/sec

$\widetilde{\omega_R}$ = Argument of Perigee, degrees

Ψ = Spin angle, degrees

ζ = Damping ratio

Subscripts

A_{AD} = Aerodynamic disturbance

A_B = Magnetic field reference

A_{BD} = Magnetic field disturbance

A_{body} = Spacecraft

A_c = External control

A_d = Disturbance

A_{frame} = Control law body reference frame

A_f = Friction

A_m = Motor

A_{net} = Sum of all forces, moments, etc.

A_R = Orbital reference frame

A_{rel} = Relative state comparison between two objects

A_s = Sun reference

A_w, A_{wheel} = Reaction wheel

I. Introduction

The CubeSat form is a size convention of small satellites that has begun revolutionizing access to space. In effect, The CubeSat concept turns the spacecraft design problem on its head. Rather than having a mission to accomplish and designing a craft to meet that functional need, the CubeSat form has a defined volume and mass limit that provides unique advantages and challenges. In his 2010 TED-X presentation "Making Space Smaller," CubeSat designer, Kiko Dontchev expressed this sentiment: "We were given a box, and we're asking the question: What can we do inside the box?"

The CubeSat parameters were developed by Stanford professor Bob Twiggs and Cal Poly San Luis Obispo professor Jordi Puig-Suari in 2000 [1]. CubeSats are defined as spacecraft with sides that measure 100 mm by 100 mm by 100 mm. These volumes can be added together to build larger satellites. CubeSat size is designated by the cube multiple followed by a U; for example, a CubeSat made up of 3 cubic volumes would be considered a "3U" satellite. Depending on deployment methods each, U can weigh up to 2 kg [2]. In a presentation at the Small Satellites and Services, "The 4S Symposium" in 2010, Greenland and Clark noted some of the features of these design constraints provide "access to more lower cost launch opportunities through standardized interfaces," utilization of modular subsystem components, and limited or no redundancy [2]. The comparatively small launch mass also means the systems tend to be considerably cheaper than their large-scale counterparts.

The general trend of material and electronic improvements has helped to allow for the miniaturization of spacecraft. The CubeSat convention is a standardization of

characteristics that allows the launch of small satellites to become a much more homogeneous affair. The standards developed allow for routinized handling and deployment of small spacecraft, which has the effect of lowering risk and mission complexity while allowing for more launches at lower cost. Recently, a number of companies catering to the development and hardware design of CubeSats have formed. For example, Blue Canyon Technologies, Clyde Space, and Pumpkin are just a few of the many new companies looking to cater to the growing niche.

CubeSats have come to be thought of as mission-risk enablers [2]. They are ideal platforms for small scale, in-situ testing of technologies that can then be further qualified and scaled. Funchal notes that these "dedicated payloads" reduce complexity and "payload-payload" conflicts. [2] also notes that low TRL (Technology Readiness Level) technologies, can be flown early in their development to help speed their maturation, helping to lower the cost and effort of putting innovative technology into orbit.

Although CubeSats have become commonplace in the aerospace world, control of their attitude is still the focus of much research. Their limited size makes designing complex control systems difficult. Much effort has gone into converting conventional means of controlling large scale spacecraft into smaller, more efficient packages for use on these miniature spacecraft. This thesis attempts to design a system that combines a number of technologies in such a way as to effectively allow for single axis control of a passively stabilized CubeSat. The preexisting platform chosen in this design is stable without concerted effort around its pitch and yaw axes; however, it freely rolls in response to its environment. A discrete control unit is developed to provide control

authority to the previously uncontrolled axis. Figure 1 has an illustration of the spacecraft axes in reference to orbit and stabilizer.

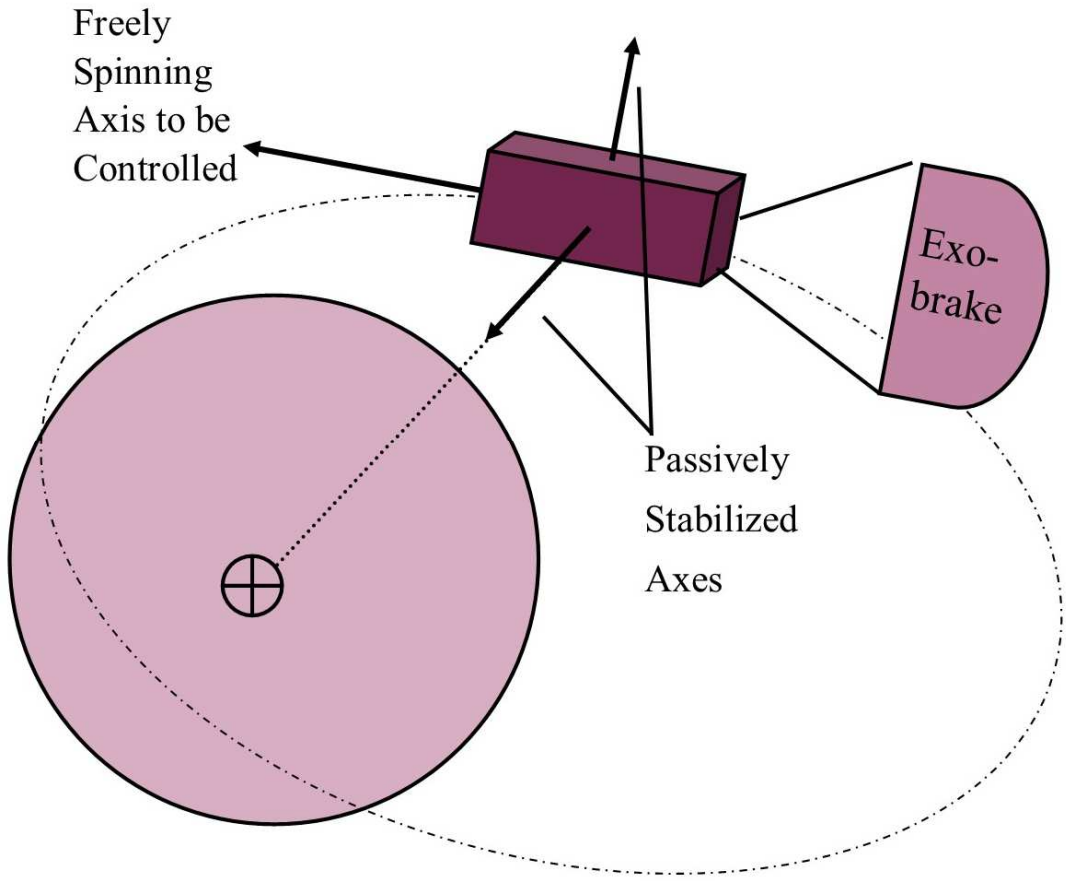

Fig. 1 Spacecraft orientation on orbit. Pitch and yaw axis stabilized by Exo-brake. Roll axis to be controlled by reaction wheels.

To meet performance requirements (developed later in this thesis), a reaction wheel and magnetorquer control system has been designed. The reaction wheel will solely handle all attitude operations, such as the de-spin maneuver for mission initialization and the station-keeping maneuvers for orientation tracking. The reaction wheel will operate until disturbance torques and friction loss saturate the wheel's momentum capacity. Once the wheel reaches 50% momentum capacity, a magnetorquer is activated to remove

the excess momentum from the system. Because of the limited accuracy of the magnetorquer, it is not used during nominal attitude operations.

For this design, the TechEdSat platform was chosen as the host operator. TechEdSat is a family of CubeSats that range from 1U to 3U. Through a NASA-SJSU partnership, faculty and students have made considerable contributions to its success.[*] Many of TechEdSat's systems were developed by aerospace and mechanical engineering students and this thesis proudly continues the technology development partnership. TechEdSat_01 is notable for being in the first group of CubeSats to be deployed from the International Space Station, ISS.[†] This study assumes the control system to be designed in this thesis will similarly be launched in a typical ISS orbit. As such, much analysis and dynamics are derived from the assumption that the orbit is circular and has the same orbital parameters as the ISS. A number of other students also developed subsystems for the TechEdSat platform during the time this thesis was written and some of their work is referenced in later parts of this thesis.

TechEdSat_03 was the first spacecraft to deploy an exo-brake, an experimental, high altitude, deorbiting device.[‡] At the time of publishing, the TechEdSat platform is currently researching the effects of high altitude deorbiting devices. In addition to quickly degrading the orbital height, one of the effects of an exo-brake is to constantly orient the spacecraft in such a way as to point its spin axis in the direction of travel. This phenomenon allows for the unique and significant assumption that the yaw and roll rates

[*] From http://techport.nasa.gov/view/11190
[†] http://www.nasa.gov/centers/ames/engineering/news/techedsat_feature.html#.VjP47berRD8
[‡] http://spaceflight101.com/spacecraft/techedsat-4/

are very small and will be assumed to be exactly zero for all analysis. While small and oscillatory in reality, the exo-brake is assumed to keep the spin axis perfectly aligned with the direction of travel. The orientation and consequences of this assumption shall be explained in detail and thoroughly discussed throughout the body of this thesis.

II. Control Strategies

While many CubeSats have taken a completely passive approach to controlling their attitude, there is great interest in developing the capability for active, precise control. In their 2013 review, Small Spacecraft Technology State of the Art (SOA), NASA scientists cited the similarities between control systems of CubeSats and their large-scale counterparts [3]. They equate the challenge of the development of Attitude Determination and Control Systems (ADCS) in CubeSats with the challenge of developing miniaturized systems that do not lose performance as they are scaled down [3].

In the field, there are many strategies for controlling spacecraft. Due to their small size, CubeSats are somewhat limited in control strategies compared with their larger relatives. Several conventional CubeSat control strategies have been considered and are introduced here.

A. Spin Stabilization

The Space Mission Analysis and Design (SMAD) handbook refers to spin stabilization techniques as "particularly simple and robust" [4]. It notes that spinning systems are often cylindrical and maintain one axis of control in the direction of their axis of spin. SMAD divides spinning satellites into three categories: passive spin, spin with

precession control, or dual-spin. Spacecraft that have no control authority over their spin are considered passive spinners. This is common in interplanetary atmospheric probes, such as Pioneer Venus, Galileo, and Huygens where mass and energy are at a premium. Satellites with control authority over their spin axis direction are known as precession controlled spinners and apply torque in a perpendicular direction to exert authority [4]. Satellites can have their entire body spinning or may be separated into discretely spinning portions for varying levels of control. A dual-spin system usually involves a spinning central mass and a 'de-spun' platform that can track a target [4].

Although many texts exist on the design and stability of spinning spacecraft, spin stabilization is not a method of control selected for this design. The interested reader is referred to Curtis' text, *Orbital Mechanics for Engineering Students,* for an in-depth development of the dynamics and stability of 'spinners' [5].

One difficulty in the utilization of spinning control methods comes from the standardized deployment methods for deploying CubeSats. Two of the common launchers for CubeSats are the P-Pod deployer and NanoRacks CubeSat deployer; both intentionally deploy satellites from torpedo-like launch tubes with little to no rotational energy. The P-Pod deployer is essentially an extruded rectangular shell with a hatch that, when open, allows for CubeSats to be deployed down a set of rails by springs [6]. P-Pods are commonly strapped to rockets and deploy their payloads only after the primary payload has been delivered on orbit. The NanoRacks deployer is functionally the same but deploys CubeSats from the ISS [7]. Unlike conventional spinning deployment

methods, which tend to launch satellites like a Frisbee, both deployers do not serve to impart any useful amount of rotational momentum.

In order to gain the benefits of a spin stabilized spacecraft, a specialized deployment mechanism would need to be created from the ground up. Designing, building, and testing, a new deployer would lose the benefits of the standardize launch mechanisms. Lee et al. presents a design methodology for a generic launcher to deploy a 20 kg satellite [8]. Their design calls for deployment by unfurling a satellite to make it spin, like throwing a yo-yo. Alternative design details are laid out by Rossoni et al., for a Frisbee-like release of a 25 kg spacecraft [9]. Their deployment mechanism is a pin and spring connector that forces the satellite to rotate around a pivoting hinge joint. It is clear that these deployment mechanisms were developed at considerable effort and expense.

B. Gravity Gradient

Gravity gradient control is a common passive approach to maintaining a nadir pointing spacecraft. When distributed masses are properly oriented in a spacecraft, the forces of gravity can be used to cause the spacecraft to always point toward the center of Earth. Its simplicity can be an attractive quality to small satellite manufacturers.

Gravity acts as an attracting field that becomes more intense the closer two bodies are. Although the effect may be slight, a rigid body that has a properly distributed mass will experience more forces on the part of its mass closest to Earth's surface. These forces will tend to "pull" the lower portion of the body toward Earth as the bottom of the spacecraft tries to "fall" to a lower orbit while the upper portions of the spacecraft are not affected to as great an extend. This tendency creates an internal stretch of the spacecraft

has the effect of constantly reorienting the body's "feet" toward and its "head" away from the ground.

If the body is properly designed, this effect can be strong enough to reject disturbances and maintain its orientation toward Earth's nadir [5]. The forces can be quite substantial. For example, in LEO, the Space Shuttle experienced gravitational torques on the order of 1 N·m [5]. All non-symmetric bodies will experience this torque in a gravitational well. Though this force can be considered negligible in certain applications, it is present in all missions and must be accounted for as a disturbance torque if not utilized as a control strategy.

This form of control can be ideal for a 3U spacecraft, because of their elongated length. In a study published by Erich Bender, a Cal Poly Sat Luis Obispo student, analysis showed that a 3U CubeSat using a set of masses on extended booms could expect to have nadir pointing accuracies on the order of half a degree [10].

C. Thrusters

The use of reaction control system (RCS) thrusters is commonplace among conventional satellites. Thrusters utilize the concept of action-reaction pairing to receive an equal and opposite force when they expel small amounts of mass at high velocities.

To date, no known CubeSats have flown RCS thrusters. The 2013 NASA SOA cites that limitations in size mass and power make thrusters an unattractive option when compared with the widespread use of magnetorquers in LEO [3].

For the foreseeable future, RCS thrusters are not likely a control option for small CubeSats. Further understanding of their control can be found in Curti's Lyapunov-

control based thrusters paper [11]. The control methodology used by [11] is to switch RCS thrusters on and off at given time intervals to linearly control spacecraft for real time control. It is notable for future use on CubeSats because of the method's low computational load, which is desirable for the limited computing power of CubeSats.

D. Reaction Wheels

Spinning objects, such as spacecraft and bicycle wheels, have angular momentum. A reaction wheel utilizes a motor to spin a discrete mass independently of the rest of the vehicle. Since the wheel is physically connected to the spacecraft, the laws of conservation of momentum dictate that momentum can be transferred between the two [5]. The momentum exchanged between spacecraft and wheel allows for precise control of the spacecraft along the spin axis of the wheel [5]. Over time, a spacecraft will tend to gain rotational momentum from outside disturbances. To reject these disturbances, a reaction wheel can be commanded to change its spin rate. This creates an equal and opposite amount of momentum, which allows the spacecraft to maintain orientation. Eventually a spin-speed limit is reached and the wheel becomes saturated. When this occurs the wheel loses control authority until its speed can be sufficiently reduced. Therefore, spacecraft need a secondary system to shed their excess momentum [4]. Curtis notes that reaction wheels excel at rejecting sinusoidal disturbances, which wax and wane repetitively over orbital periods [5].

Recent advances in reaction wheel technology make reaction wheels an attractive control option for CubeSats. [3] cites numerous wheels with CubeSat "flight heritage"[§]. Compared with other actively controlled systems, reaction wheels tend to be relatively light and require low power [3].

Valdemir Carrara and Helio Kuga have developed close-loop, negative-feedback control of a reaction wheel for a one degree of freedom platform model [12]. Their work improves motor models and accounts for static and rolling friction of the wheel when in different states of motion. This project draws on their performance parameters to design a reaction wheel system.

Sidi published a spacecraft control book that has been instrumental in development of the control laws and reaction wheel dynamics used in this thesis [13].

E. Magnetorquers

Electricity that is moving through a wire creates a weak magnetic field. In a frictionless environment, a magnetic spacecraft can interact with Earth's magnetic field to exert controllable torque on spacecraft. This is the basis for a simple, lightweight controller known as a magnetorquer. Although the dynamic equations of motion are complicated, there is considerable attractiveness in the simplicity of the actuator. Coils of wire can be wrapped around themselves to create an effective device—no moving parts or propellant required. Wang et al. presents a paper that lays out the dynamics and

[§] Flight heritage is a term that refers to the concept of reusing component designs from previous flights. A standardized car battery, for example, has extensive flight heritage (for cars). If you were designing a car, you'd probably consider buying someone else's design for a car battery rather than develop a whole new one. The same is generally true for spacecraft. Spacecraft manufacturers try to limit the expense of development and testing by choosing to reuse components that have extensive flight heritage.

equations for control about all three axes of a spacecraft [14]. Because of the time varying nature of the magnetic field strength that is experienced by the spacecraft, a magnetometer must be used for exact measurements of local field strength. It should be noted that magnetorquers rely on operation in relatively strong magnetic fields, such as Earth, and will not properly function in deep space or around planets without magnetic fields.

This actuator is a key strategy for a number of CubeSats that have flown in space. This may be because of the relative simplicity of the magnetorquer hardware and the low volume/power requirements. The widespread use of this technology also has the effect of giving magnetorquers a high flight readiness level, specifically for use on CubeSat missions. Indeed, [3] reviewed 3 magnetorquers that had reached a Technology Readiness Level of 9/10, showing considerable flight heritage and success.

III. System Design Parameters

As per best practices, the design process is guided by a systems engineering approach. Systems design is a design approach that highlights the interconnectedness of subsystems and focuses on balancing the optimization of the design against the requirements of the system as a whole. The first steps taken were to identify key drivers of the TechEdSat system and to identify the requirements that the system must achieve in order to meet the performance parameters developed by Eddie Uribe, a student and team lead of a small group of SJSU engineers investigating new projects for the TechEdSat. The requirements are multi-tiered so as to describe levels of successful mission deployment. These requirements are adapted from a set of discussions which considered the

TechEdSat's current performance capabilities and outline the parameters for performance improvement. They can be found in a preliminary mock proposal for launch with a launch provider and are recorded below:

- Develop a flight system to be ready for hardware delivery. Launch date not set. This system should be minimal and only engineered to achieve the highest level of mission success criteria.
- Demonstrate the ADCS and achieve a TRL of 7.
- Enable active control about the spin axis to allow for its stabilization.

The outcome of the mission will also be assessed by how well it meets success criteria. The most desirable outcome will be to achieve maximum success; however, the mission would be well-received if it can meet the minimum level of success. Those tiers are defined below:

- Minimum Success – Demonstrate a level of attitude control over the spacecraft. This will consist of having the capability to initialize a newly-designed ADCS system and to successfully modify the momentum of the spacecraft.
- Medium Success – Achieve full attitude control over the spin axis of the spacecraft. This will consist of successfully detumbling the spacecraft, demonstrating a 'hold position' maneuver, and successfully pointing a body-mounted payload at Earth's surface.
- Maximum Success – Achieve Earth pointing capabilities and demonstrate momentum rejection with magnetorquers over the course of several cycles.

An internal requirements document has been created to consider the effects of the performance requirements. This document is intended to account for important performance parameters and will serve as a guide for the development of the system. In bulleted form, these requirements lay out all tasks that the spacecraft must be able to perform.

- article to be pointed
    - optical payload
    - comms antenna
- pointing direction
    - Earth's nadir
- pointing range – possible pointing directions
    - Earth's surface at Earth-based ground stations
- pointing stability
    - constant or reliable target acquisition
    - 1^{o} of accuracy
- power limitations
    - system should run on a 2.5 Watt, 5 V microprocessor
- slew rate
    - sufficient speed to complete roll maneuver in a reasonable amount of time
- exclusion zones
    - none specified
- communications antenna pointing

- antenna should face nadir within 1° when communicating with Earth

- pointing during thrusting
  - no propulsion system, no control needed

IV. Trade Study

A trade study was performed to explore the 3U CubeSat design space and to choose an appropriate actuator subsystem to meet the internal requirements. Table 1 shows the results of the trade study. This study considers 7 alternatives for pointing authority and weighs their characteristics versus the perceived value to the mission to reach an informed decision. The reaction wheel and magnetorquer combination is the highest performer. A sensitivity study is also presented to help to understand the effect of varying the weights of each characteristic. The magnetorquer and reaction wheel combination consistently ranks among the highest, if not the highest, subsystem.

Table 1 Trade study of actuator architectures. Magnetorquers and reaction wheel were found to be a strong control strategy.

Parameter	Weight (1-5)	Magnetorquers	Dual Spin	Thrusters	Magnetorquers + Reaction	Thrusters + Reaction	Gravity Gradient + Magnetorquers	Spin Stabilized
Ability to meet pointing req	5	8	10	10	10	10	1	4
Mass	4	10	8	2	7	1	10	10
Complexity	4	10	7	2	6	3	9	9
Power	2	9	8	3	7	1	9	10
Accuracy	5	6	6	10	10	10	5	6
Poitning Authority	3	5	3	10	10	10	4	0
TRL	4	9	5	2	7	1	9	8
Deployablity	2	10	2	10	10	10	9	2
Fault Recovery	2	4	0	7	9	9	5	0
Totals		**247**	**189**	**194**	**262**	**190**	**200**	**182**

Variants							
Base	247	189	194	**262**	190	200	182
performance high, for tight budgets	263	204	191	**266**	185	214	201
high performance, for loose budgets	237	165	216	**266**	212	189	150
COTS: smple, pnting req unimportant	**260**	167	163	243	156	232	185
focus on doing what's been done	235	156	175	**237**	168	201	163

Other actuator subsystems, while each having their own benefits, have certain restrictions or difficulties. For example, many CubeSats that use active ADCS employ

magnetorquers exclusively to control their attitude, which are well defined and have been used extensively by CubeSats. They are lightweight and robust: they can be as simple as a coil of wire and a battery connected together to create a magnetic dipole. Unfortunately, they do not have a high degree of precision and have a slow response to perturbations.

Similarly, dual-spin and single-spin stabilized crafts are attractive alternatives from an upkeep and control stand point. They also have extensive flight heritage among large scale satellites. Their difficulty, however, comes in deployment. Spin stabilized CubeSats have yet to be used for attitude control; to date, there is only one known CubeSat in development that utilizes a dual-spin control method [15]. Its use was only for payload articulation and did not serve to give the CubeSat attitude control authority [15]; a similar method might have been used to aim the antenna or payload of the TechEdSat system.

Next, though gravity gradient is extensively used for 3U satellites for nadir-axis control, satellites that use gravity gradient stabilization tend to have low accuracy. As discussed previously, the control method uses gravity to pull the bottom of the spacecraft to face Earth's center and can be likened to grasping a pen by its tip and dangling it above a table. It is conventionally a passive system that does not readily allow for an intentional change in orientation. Because integration of the TechEdSat anticipates the antenna and payload to be fixed to different surfaces, it must be able to actively change its orientation and thus does not meet pointing requirements for this mission.

Finally, although thrusters are highly accurate for 3-axis control, they were rejected from this thesis because of their several deficiencies. Thrusters must house and spend a finite amount of reaction mass to control spacecraft orientation. Even if the micro-satellite RCS technology had matured past infancy, there exist great concerns about putting any form of propellant on a secondary vehicle while inside a launch vehicle (not to mention in an enclosed environment like the ISS). If a catastrophic failure of the low-cost CubeSat occurred, a multi-million-dollar primary mission could be damaged or lost. The TRL is also considerably lower than that of any other control architecture because of the complete lack of flight heritage of micro-scale thrusters. Although there are many missions in development and while it may be commonplace 3-7 years from now, there are currently no examples of CubeSat thrusters having been successfully flown [3].**

Thus, a combined reaction wheel and magnetorquer scheme is the best design path for this study. It gains the benefits of high precision authority from the reaction wheels and the momentum changing capability of magnetorquers. Although the combination of these two systems will undoubtedly increase the complexity and cost of the design, the added capability will enhance the overall effectiveness of the TechEdSat system. Additionally, the system will have limited redundancy because the spin axis will have two actuators to rely on; if the reaction wheel fails, it is expected that the magnetorquer could be rigged to give limited control authority. The system is designed to be modular and could be deployed in multiples in the future for active control in all 3-axes.

** This includes one project by an SJSU Graduate, Ricardo Amezquita, developing a 1U thruster module for use on large-U CubeSat systems.

To verify the robustness of these results, a sensitivity study was developed. The weight of each control characteristic was varied to evaluate how the overall score changed as criteria were valued differently. The original trade study placed a high value on the ability to acquire a target to a high accuracy and secondarily valued mass, power, and technology readiness level (TRL). The second test valued the 4 previous criteria equally, and discounted the rest. The third test devalued mass, power, and complexity requirements, while highly valuing deployability and the TRL. The fourth test was an attempt to quantify a "simplistic" system that had controllability but did not need to meet the pointing requirements; it highly valued low cost (assuming complexity correlated with cost) and high TRL. The final test devalued many categories and focused on TRL and deployability alone. The results of all but one of these tests found that the combination of magnetorquer and reaction wheel is the ideal choice. The sole test that did not score reaction wheel and magnetorquer package as the highest valued option scored it as a close second behind solely using magnetorquers. Due to sensitivity consistency, magnetorquer and reaction wheel package is believed to be the ideal architecture to pursue in this mission design.

V. Architecture

The ADCS system is designed to meet mission requirements for ground observation. To meet those needs, while maintaining a low-cost budget, ADCS will be built from the ground up, rather than purchasing a costly pre-fabricated system. The system is broken into three subsystems: sensing, actuation, and a controller. This can be seen in Fig. 2.

All ADCS components will be tied to a subsystem microprocessor which will handle control commands, spacecraft dynamics, and package state information to be output.

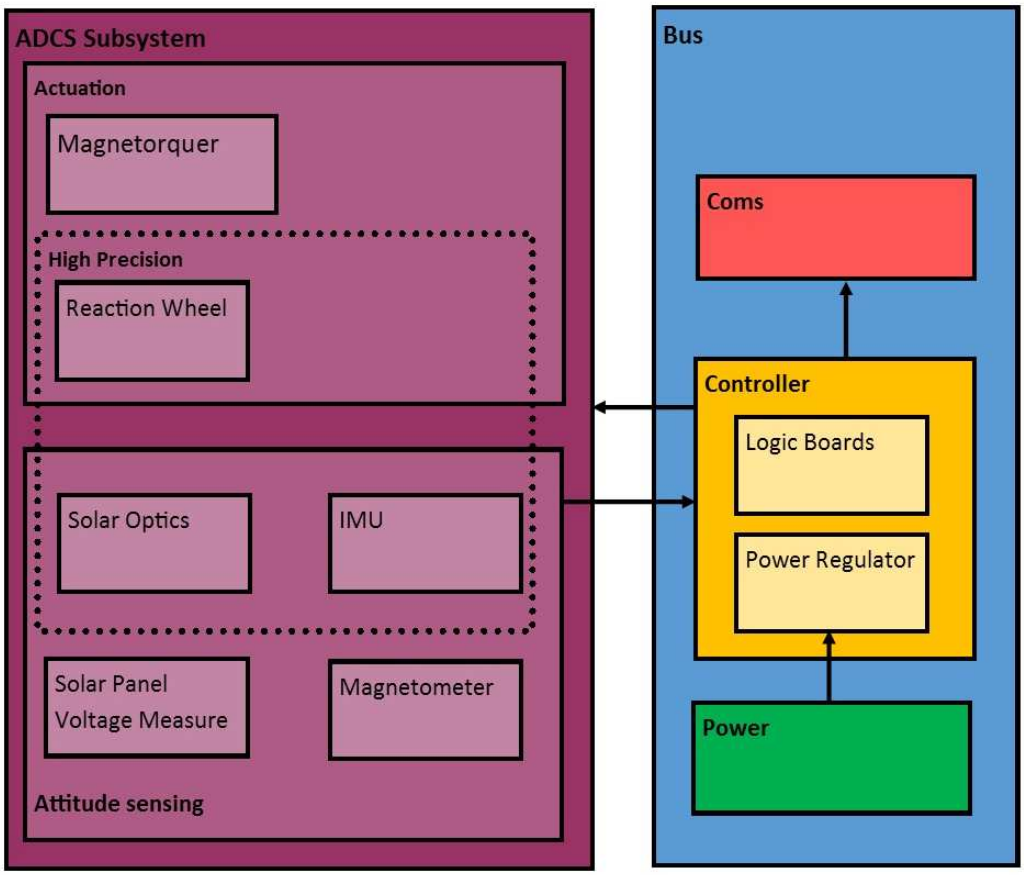

Fig. 2 Layout of ADCS architecture for visual reference. The components of the system will utilize commands from the C&DH system to achieve a pointing solution.

Through architecture considerations and trade study, spin-axis control will be achieved with the use of reaction wheels for fine pointing control. The reaction wheel will enable high-precision pointing until a predefined level of saturation is reached. If fully saturated, pointing authority will be lost. Magnetorquers will desaturate the wheels to acceptable levels to maintain authority.

A logic control board hosting control software will be developed in-house as part of the C&DH system and will be required to drive spacecraft attitude. Preference to the Intel Edison microprocessor has been given by the TechEdSat team and is expected to be used in a possible prototype of this design.

This controller will determine the TechEdSat's attitude and direct torque to properly align the craft to its target. It will be required to process the optical images for high-precision attitude knowledge. It will also output attitude measurements to the Coms sub-system for ground transmission.

A. TechEdSat Architecture Considerations

The TechEdSat platform has been chosen because of the synergies between its control goals and the goals of this project. The TechEdSat is a family of CubeSats developed jointly by NASA Ames engineers and San José State University students and faculty. Recent flights of the TechEdSat_3 and TechEdSat_4 have utilized a deployable apparatus that works as a parachute to create enough drag to slow atmospheric reentry enough to reduce the need for advanced heat shielding systems to protect the spacecraft.

The exo-brake also serves as a means to utilize atmospheric torques to passively stabilize the spacecraft in orbit. The stabilization occurs in the set of planar axes perpendicular to the flight path. In other words, it tends to stabilize the pitch and yaw axes of the spacecraft while allowing TechEdSat to freely rotate around its spin axis.[††] If the moments generated by the atmosphere are enough to overcome the gravity gradient,

[††] Discussion with TechEdSat's Primary investigator, Marcus Murbach.

solar pressure, and magnetic moments, the spin axis will be constantly aligned with the velocity vector.

B. Sensor Strategy Overview

Attitude determination will be performed by a number of sensors to define the body frame in the Earth Centered Inertial frame. Reference frames will be explained in detail in a later section of this thesis. Orientation will be determined with Earth sensors and a magnetometer in the reference frame. Body rotation rate will be found utilizing an IMU.

Early work on this project considered solar tracking with optical equipment. That work analyzed knowledge requirements which have been preserved here in the interest of possible future developments. 3-axis control can only be achieved when two unique vectors relative to the spacecraft body are defined. An ADCS system tracking the sun could locate the sun through a two stage, coarse-fine, process. Previous work envisioned sun sensors to give general knowledge of the sun's location relative to the body frame. At nearly 150 million kilometers, the sun is a two-thirds-of-a-degree target. Once located with sun sensors, the control system would drive the sun normal to the face of the CubeSat with 1^{o} to 2^{o} of accuracy. Once alignment is reached, the CubeSat could use a special optical package to resolve the sun's location to a high degree. A control algorithm would process the optic image and get knowledge of the sun's location to hundredths of a degree of accuracy. The control system would then be used to drive the CubeSat's face to be completely normal to the sun and body rates would be measured to maintain tracking over time.

Previous work suggested sun sensors would be a viable strategy for attitude determination. Although they are not expected to be used in determining TechEdSat's attitude, the research done on them has been preserved here. Sun sensors can be broken into two categories: coarse and fine sensing [3]. Fine sun sensors can reach accuracies of up to 0.1° [3]. Coarse sun sensors have accuracy on the order of several degrees [4].

In the event of sensor failure, sun location and thus orientation could be determined (to an extent) by tracking solar cell voltage. The efficiency of solar cell performance is a function of solar cell incidence angle to the sun and are most efficient when positioned normal to the sun. Since cells will be face mounted, the highest voltage reading taken by the cells would indicate the closest angle to sun-facing orientation. If the sun's orientation to the satellite can be determined, the sun pointing angle can be used to find the CubeSat's absolute attitude on orbit based on a solar reference model. Ideally, the model would determine the location of the sun in the Earth Centered Inertial Fixed frame and could be used as a reference to determine body frame orientation. Such a model will not be developed in this thesis.

C. Block Diagrams for ADC Sub-system

The layout of the system has been drafted and serves to highlight some of the higher level aspects of what the system is designed to do and shows the interconnected nature of the pointing system to the rest of the satellite. These diagrams were developed with reference to "Development of Attitude Determination for Student Pico-Satellite INNOSAT," which is a paper that lays out the design of the INNOSAT CubeSat's

attitude sensing block diagram [16]. The model of their attitude determination process was adapted to meet TechEdSat's attitude determination needs, shown in Fig. 3.

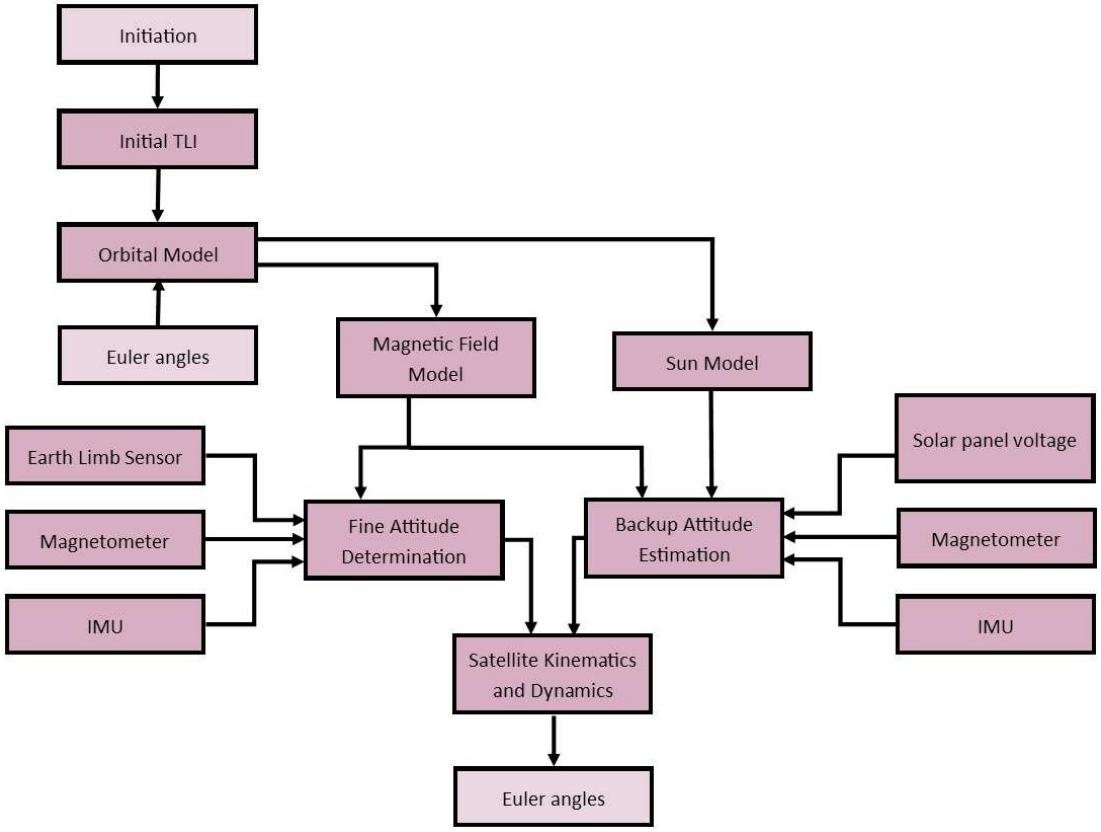

Fig. 3 Attitude sensing strategy under nominal operation. The attitude determination software must be able to function in eclipse and in view of the sun. If the position sensor were to fail, knowledge of voltage generated by solar panels can be used to estimate position.

The attitude determination diagram lays out the sensors used in both the nominal operation and backup operation. In either eclipse or sun view, the position on orbit can be determined by an Earth limb sensor package. Body rotation rates can be sampled with an IMU and the magnetic field can be measured with a magnetometer. All this information is taken into account when determining how much control effort to exert with the actuators to achieve desired pointing results. If the Earth sensor fails, some

degree of pointing knowledge can be maintained by searching for the maximum voltage on solar panels to estimate the spacecraft's orientation to the sun. Based on the knowledge that the spacecraft will go into eclipse, the backup sensing strategy of using solar panels to find a sun pointing angle will not always be possible. A Kalman filter can be used to estimate the Earth's limb or the sun's location to maintain a nominal estimation of position during times without direct measurement from these sensors [16]. In this case, an estimation of the satellite's attitude would be used until the spacecraft comes out of eclipse or is able to re-acquire the Earth's limb.

With knowledge of the Earth-spacecraft references, torqueing control will be exerted by the satellite to precisely point at its target. Utilizing a use-what-you-have approach, the high-accuracy reaction wheel will control the spacecraft's attitude to point toward the sun and to reject orbital disturbances at all times. Figure 4 lays out a block diagram that depicts the nominal operational capabilities of the ADCS.

Even though reaction wheels have many benefits, their capacity for momentum storage is not infinite. Eventually, their motors will spin so fast that they will reach a saturation limit. This limit may be due to the maximum torque they can exert on the wheels, the vibration they induce into the system, or the limit of power that can be delivered to them. Their eventual saturation will cause a loss of authority to control the spacecraft. When this occurs, the secondary control system will engage. A magnetorquer will exert a magnetic moment that interacts with Earth's magnetic field to create a torque on the spacecraft. This torque will be equal and opposite to the moment created by the reaction wheel as the wheel is slowed down. Eventually, through this

interaction, the momentum wheels will be brought to some nominal speed and can resume normal operation.

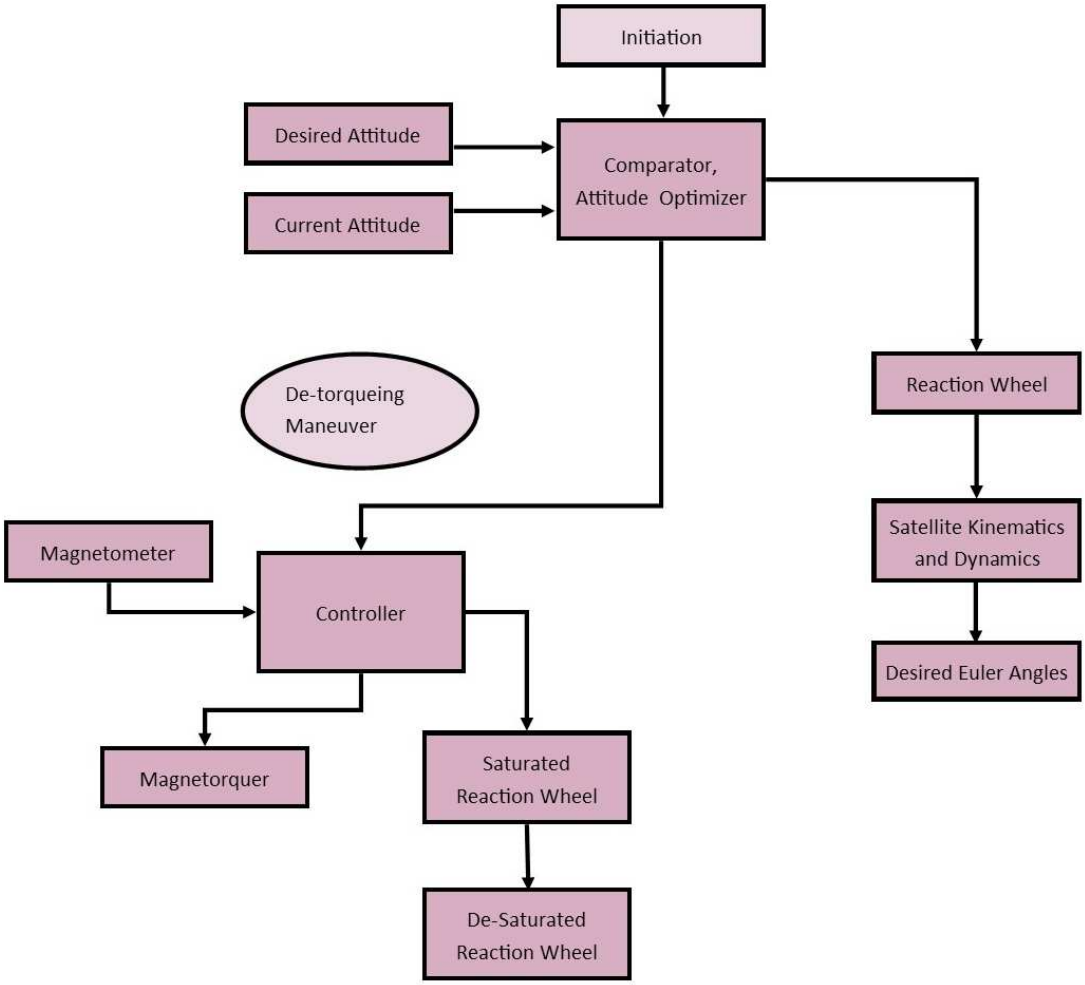

Fig. 4 Attitude control strategy under nominal operation. The control operations are broken into two operational abilities: control attitude with reaction wheel and to desaturate reaction wheel with the magnetorquer.

VI. Reference Frames

Orbital motion is rarely intuitive. When considering objects moving through space, it is often instructive to define a set of convenient reference frames and relate separate frames to each other through transformations. Reference frames are a set of 3 orthogonal

vectors defined by relation. The first vector is specified by requirement, the second is set by preference, and the final vector is defined by its perpendicularity to the other two and positive in a right-hand-sense [17].

A. Earth Centered Inertial Frame (ECI)

The ECI frame is located at the center of Earth's mass and does not change its orientation over the timespan of a mission. The "X" vector comes out of the equator and points toward the vernal equinox. The "Z" vector is defined to point in the direction of Earth's rotation vector, which can be visualized as a line coming out of the North Pole. "Y," the third vector, is orthogonal to both [17]. The sun is included in the model to help the reader visualize the reference frame. Though the Earth revolves around the sun, in reality, there is no mathematical difference between modeling the Earth moving around the sun or the sun around the Earth. In this frame, the spacecraft and sun are both modeled as bodies rotating around a non-moving (inertial) Earth. This is visualized in Fig 5.

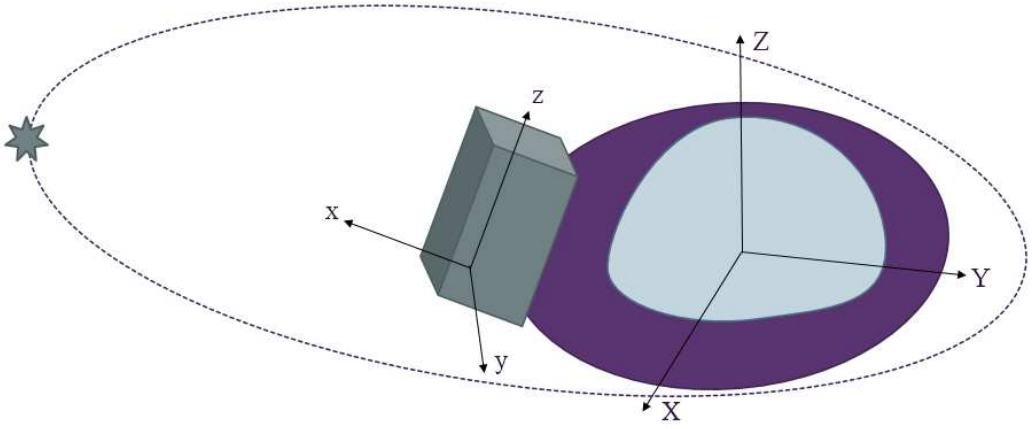

Fig. 5 Diagram of ECIF, satellite, and sun rotating around inertial center.

B. Body Frame

The spacecraft body frame is a set of vectors attached to the body of the spacecraft [17]. This allows the frame to rotate with the spacecraft. The frame's origin is located at the center of mass to simplify rotational characteristics of the body in free-space. Under rigid-body conditions, each discrete component of the spacecraft can be defined by vector from the spacecraft's center of mass and does not change with respect to time.

Following the convention outlined previously, TechEdSat's body frame origin lies at its center of mass. The "x" vector points normal to the spacecraft's primary face. This face will track the nadir during payload operations. The "z" vector will point along the length of the CubeSat's extruded body and points in the direction that the spacecraft will be traveling. The "y" vector will be defined as an axis perpendicular to both the "x" and "z" vectors as shown in Fig. 6. An ideal design would allow the principle axis to align directly with the chosen coordinates, such that all products of inertia vanish. This will be discussed in further detail later in this thesis. The TechEdSat is designed such that the exo-brake deploys from the bottom of the CubeSat, in the negative "z" direction.

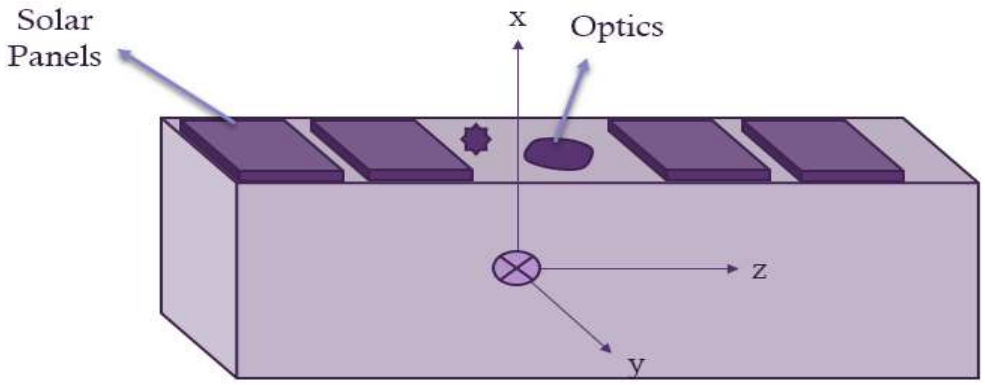

Fig. 6 Body reference frame, attatched to center of mass of TechEdSat.

C. Orbital Reference Frame

A conventional approach to orienting the spacecraft is to reference it to the orbital reference frame. This frame travels with the spacecraft, like the body frame, and is located at the center of mass of the spacecraft [13]. Unlike the body frame, the coordinate frame is not fixed to the spacecraft; instead, the coordinate frame is developed with respect to Earth and the spacecraft's orbit. The z_R-axis, denoted by an 'R' for reference, is fixed to point toward Earth's center of mass. The x_R –axis lies in the orbital plane and points in the direction of its orbital velocity (commonly referred to as its 'ram direction'). The y_R – axis completes the right-hand coordinate frame by being orthogonal to both x_R and z_R [13].

VII. Rotational Kinematics and Dynamics

As the CubeSat hurtles through space, its motion will follow well-defined physical principles that can be measured and controlled. The following section describes the kinematic motion of orbiting bodies and explains necessary mathematics to describe the relationship between the body and inertial frame. Spacecraft motion is tracked by its location at a given time [5]. While an understanding of linear motion will allow the reader to make direct associations to rotational motion, it is not a focus of this paper's design problem and will not be explained in depth. Interested readers are directed to [5] or [13] for a full discussion of linear motion.

A. Kinematics

Kinematics are the mathematical descriptions of geometries changing in space over time. Kinematic equations also allow for the relation of reference frames and allow for

the transformation of known quantities in one frame into a more useful frame for analysis. This relationship is especially important when considering the motion of rotating bodies in space. Newton's well-understood laws of motion apply only in inertial space [5].

In order to utilize the laws of motion, vector quantities, such as position or velocity, of a spinning body must be related back into the inertial frame. To relate two frames, the fundamental kinematic equation must be utilized. This equation states that the time rate change of a vector in one frame is equal to the rate change of the vector in the second frame plus the cross product of rate of change of the second reference frame relative to the first and the original vector. An example of this equation can be seen in Eq. (1)

$$\dot{\boldsymbol{r}}_{\boldsymbol{A2}} = \dot{\boldsymbol{r}}_{\boldsymbol{A1}} + \boldsymbol{\omega}_{\boldsymbol{A1A2}} \times \boldsymbol{r}_{\boldsymbol{A1}} \tag{1}$$

where the rate change of a position vector is considered between some *A1* and some *A2* frame.

B. Magnetic Field

The magnetic field used in this paper is a simplified model of the magnetic field surrounding Earth. While the magnetic model does a sufficient job of characterizing some of the properties of Earth, it cannot give a detailed or precise account of the field to the precision of high-resolution models. Sidi presents the model in their text on spacecraft control, which is a reference to McEvlain's 1962 model that relates the vector components of the local magnetic field anywhere around Earth to the orbital reference frame [13]. It is presented here as Eq. (2)

$$\begin{Bmatrix} B_{xR} \\ B_{yR} \\ B_{zR} \end{Bmatrix} = \frac{B_e}{{R_o}^3} \begin{bmatrix} \cos\left(\widetilde{\omega_R} + \widetilde{\theta_R} - \eta_B\right) \sin \xi_B \\ \cos \xi_m \\ -2 \sin\left(\widetilde{\omega_R} + \widetilde{\theta_R} - \eta_B\right) \sin \xi_B \end{bmatrix} \quad (2)$$

B_e is the dipole strength of Earth, taken to be 7.96e15 Tesla [4]. R_o is the orbital distance of the spacecraft to the center of the Earth, which can be taken as 6.778e3 km [5] and corresponds to a 400 km altitude. To locate the spacecraft on orbit inside the field, classical orbital elements, $\widetilde{\omega_R}$ (the argument of perigee), and $\widetilde{\theta_R}$ (the True Anomaly), are added together. The argument of perigee is the angular location of the point of closest approach with respect to the inertial "X" axis. This paper will only consider circular orbits, which give trivial location of perigee; therefore, $\widetilde{\omega_R}$ will be 0º for all analyses. The True Anomaly is the angle of the spacecraft from its perigee and spans from 0º to 360º in the orbital plane. Angular distance of the ascending node from the geomagnetic equator is η_B. Because this value acts as a phase delay to the orbit, it is satisfactory to assume that the ascending node and the geomagnetic equator align; therefore, η_b will be taken as 0^o for all analyses. The ξ_B is the inclination of the orbital plane to the magnetic equator. Earth's magnetic pole does not align with its spin axis. The recent NOAA survey, World Magnetic Model 2015, puts the geomagnetic pole at about 86º North [18]. This can be seen in Fig. 7. Because it is expected that the TechEdSat will be deployed from the ISS, its inclination will match the ISS, which is at 51.6º. Then, ξ_B becomes the sum of the inclination and angular distance of the poles, which is 56.6º.

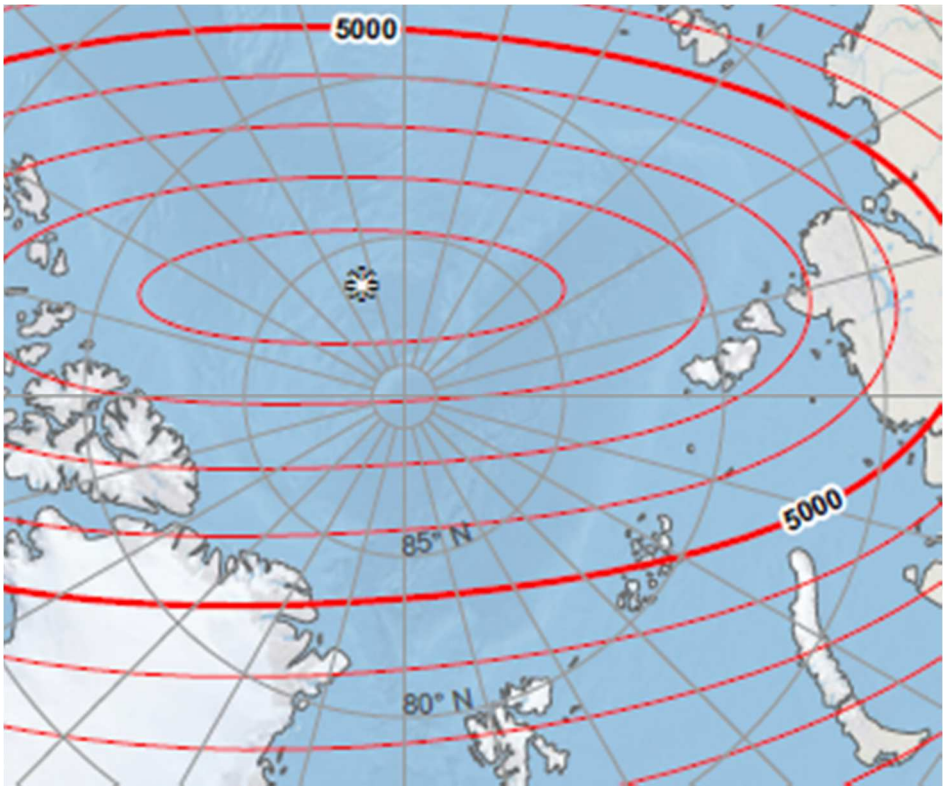

Fig. 7 Snapshot of the magnetic field location with reference to Earth's north pole. The * denotes location of the magnetic pole. This image is in the public domain.

C. Euler Angles

A common set of angles that describe a spacecraft's body frame in relation to the inertial frame is known as the Euler Angles. The transformation it describes is a set of three specific rotations to transform a vector in the inertial frame into the body frame [5]. This means that some 3x3 transformation matrix, $[\boldsymbol{Q}]_{Xx}$, can be used to translate a vector, $\boldsymbol{v}_{XYZ}$ in inertial coordinates into body frame $\boldsymbol{v}_{xyz}$ as shown in Eq. (3),

$$\boldsymbol{v}_{xyz} = [\boldsymbol{Q}]_{Xx}\boldsymbol{v}_{XYZ} \tag{3}$$

Its inverse can be performed to return a vector from the body frame into inertial. First, a rotation is made around the inertial "Z" axis, then a rotation is made about the newly

moved “x” axis, and finally, another rotation is made about the now-aligned “z” axis. Colloquially, this is known as a 3-1-3 transformation. By convention, the first rotation angle is the precession angle φ, the second is the nutation angle θ, and the third is the spin angle ψ. Each rotation can be made by multiplying the vector by an appropriate direction cosine matrix.

Direction cosine matrices are orthogonal transformations of vector components that perform a 1:1 transformation of a vector from one coordinate frame to another; proof can be found in [5]. The general equation for a direction cosine matrix can be seen in Eq. (4),

$$[\boldsymbol{Q}]_{xx'} = \begin{bmatrix} \widehat{\boldsymbol{\imath}'} \cdot \hat{\boldsymbol{\imath}} & \widehat{\boldsymbol{\imath}'} \cdot \hat{\boldsymbol{\jmath}} & \widehat{\boldsymbol{\imath}'} \cdot \widehat{\boldsymbol{k}} \\ \widehat{\boldsymbol{\jmath}'} \cdot \hat{\boldsymbol{\imath}} & \widehat{\boldsymbol{\jmath}'} \cdot \hat{\boldsymbol{\jmath}} & \widehat{\boldsymbol{\jmath}'} \cdot \widehat{\boldsymbol{k}} \\ \widehat{\boldsymbol{k}'} \cdot \hat{\boldsymbol{\imath}} & \widehat{\boldsymbol{k}'} \cdot \hat{\boldsymbol{\jmath}} & \widehat{\boldsymbol{k}'} \cdot \widehat{\boldsymbol{k}} \end{bmatrix} \tag{4}$$

$[\boldsymbol{Q}]_{xx'}$, a general transformation matrix, relates the vector components of one frame to the components of another with dot products. When rotations are computed about an axis, the direction cosine matrix becomes a set of trigonometric equations in matrix form. Because the axis about which the rotation is happening does not change orientation, its magnitude remains constant [5].

The set of three Euler rotations are described by three sequential transformations through cosine matrixes as seen in Eqs. (5-7):

$$[\boldsymbol{Q}(\varphi)] = \begin{bmatrix} \cos\varphi & \sin\varphi & 0 \\ -\sin\varphi & \cos\varphi & 0 \\ 0 & 0 & 1 \end{bmatrix} \tag{5}$$

$$[\boldsymbol{Q}(\theta)] = \begin{bmatrix} 1 & 0 & 0 \\ 0 & \cos\theta & \sin\theta \\ 0 & -\sin\theta & \cos\theta \end{bmatrix} \tag{6}$$

$$[\boldsymbol{Q}(\psi)] = \begin{bmatrix} \cos\psi & \sin\psi & 0 \\ -\sin\psi & \cos\psi & 0 \\ 0 & 0 & 1 \end{bmatrix} \tag{7}$$

Because the order of matrix multiplication is significant, these transformations must be carried out in proper sequence, as shown in Eq. (8),

$$\boldsymbol{Q}_{Xx} = [\boldsymbol{Q}(\psi)][\boldsymbol{Q}(\theta)][\boldsymbol{Q}(\varphi)] \tag{8}$$

Q_{Xx} denotes a transformation from inertial frame into body frame. These three direction cosine matrices can combine into a single massive direction cosine matrix as shown in Eq. (9),

$$[\boldsymbol{Q}_{Xx}] = \begin{bmatrix} -\sin\varphi\cos\theta\sin\psi + \cos\varphi\cos\psi & \cos\varphi\cos\theta\sin\psi + \sin\varphi\cos\psi & \sin\theta\sin\psi \\ -\sin\varphi\cos\theta\cos\psi - \cos\varphi\sin\psi & \cos\varphi\cos\theta\cos\psi - \sin\varphi\sin\psi & \sin\theta\cos\psi \\ \sin\varphi\sin\theta & -\cos\varphi\sin\theta & \cos\theta \end{bmatrix} \tag{9}$$

Because the matrix is orthogonal, it can be inverted to transform a vector from body frame into the inertial frame [5]. Though the number of trigonometric functions can be computationally intensive, simply multiplying any vector in inertial frame by the Euler transformation, $[\boldsymbol{Q}_{Xx}]$, will transform it into the spacecraft body frame.

When the rate of change of the body frame is needed, the derivative of $\varphi,\ \theta,$ and ψ can be taken. The angle rates, respectively are known as precession rate ω_p, nutation rate ω_n, and spin ω_s. The body frame rotations are expressed in Eq. (10),

$$\omega_p = \dot{\varphi}\ , \omega_n = \dot{\theta}\ , \omega_s = \dot{\psi} \tag{10}$$

[5] provides a derivation of the angular velocities in the Euler angle rates:

$$\omega_x = \omega_p \sin\theta \sin\psi + \omega_n \cos\psi \tag{11.1}$$

$$\omega_y = \omega_p \sin\theta \cos\psi - \omega_n \sin\psi \tag{11.2}$$

$$\omega_z = \omega_s + \omega_p \cos\theta \tag{11.3}$$

These equations can be solved in terms of the precession, nutation, and spin rates [5] to find the rate change of the Euler angles, as seen in Eqs. (12.1-12.3)

$$\omega_p = \frac{1}{\sin\theta}\left(\omega_x \sin\psi + \omega_y \cos\psi\right) \tag{12.1}$$

$$\omega_n = \omega_x \cos\psi + \omega_y \sin\psi \tag{12.2}$$

$$\omega_s = -\frac{1}{\tan\theta}\left(\omega_x \sin\psi + \omega_y \cos\psi\right) + \omega_z \tag{12.3}$$

When tracking the time rate change of the body frame, one must take care to avoid rotating the nutation angle through 90° to avoid the singularity that exists in the precession angle.

D. Reference Orbit to Body Frame Relation

Nominally, TechEdSat's orbit is stabilized by an exo-brake such that its z-body axis always points in its direction of travel. Control effort will be applied by reaction wheels and magnetorquers to control its orientation about its spin axis. Its nominal orientation shall be defined such that the $+x_b$ face will point in the the z_{ref} direction. The positive x_b face is assumed to have a nadir pointing payload. Counter-clockwise deviation about the spin axis from this orientation is therefore defined as a positive spin angle, ψ. To transform a vector from the reference frame into the nominal pointing direction, the orientation transformation can be written in matrix form, as Eq. (13),

$$\begin{Bmatrix} x_{b,nominal} \\ y_{b,nominal} \\ z_{b,nominal} \end{Bmatrix} = \begin{bmatrix} 0 & 0 & 1 \\ 0 & -1 & 0 \\ 1 & 0 & 0 \end{bmatrix} \begin{Bmatrix} x_R \\ y_R \\ z_R \end{Bmatrix} \tag{13}$$

The transformation from nominal body orientation can be expressed as a cosine matrix with respect to the spin angle, ψ:

$$\begin{Bmatrix} x_b \\ y_b \\ z_b \end{Bmatrix} = \begin{bmatrix} \cos\psi & \sin\psi & 0 \\ -\sin\psi & \cos\psi & 0 \\ 0 & 0 & 1 \end{bmatrix} \begin{Bmatrix} x_{b,nominal} \\ y_{b,nominal} \\ z_{b,nominal} \end{Bmatrix} \tag{14}$$

Substituting the matrices together, a transformation can be obtained from the reference frame into the body frame and is shown in Eq. (15),

$$\begin{Bmatrix} x_b \\ y_b \\ z_b \end{Bmatrix} = \begin{bmatrix} 0 & -\sin\psi & \cos\psi \\ 0 & -\cos\psi & -\sin\psi \\ 1 & 0 & 0 \end{bmatrix} \begin{Bmatrix} x_{ref} \\ y_{ref} \\ z_{ref} \end{Bmatrix} \tag{15}$$

This transformation will be utilized in considering magnetic torques operating on the spacecraft.

E. Quaternions

Mapping transformations of three dimensional space in three dimensions (i.e. Euler Angles) is a powerful and sufficient tool for most uses. There are however, certain situations where information can be lost. These singularities can happen through the division of a sine or cosine that results in a value divided by zero. Commonly, this is known as gimbal lock and can spell disaster for any attitude control system.

A mathematical convention, known as a quaternion, is commonly employed to circumvent the potential hazards of transformation singularities. Quaternions are four dimensional transformations of three dimensional space and have the unique benefit of preserving all information, no matter how they are employed.

Though they are not as tangible as Euler transformations, quaternion math in matrix form reduces the "computational burden" of onboard computing [13]. Rather than rely on a nine element matrix with multiple trigonometric functions as the Euler rotations do, quaternions are a convention that utilize linear algebra, Eigen vector theory, and complex

number theory. Quaternions describe a vector in space and an amount of rotation around that vector to model a single rotational transformation from one coordinate frame to another [13].

Quaternions are a consequence of several rules, shown in Eqs. (16.1-16.4), that define a quaternion vector, where i, j, k describe independent unit vectors:

$$i^2 = j^2 = k^2 = -1 \tag{16.1}$$

$$ij = -ji = k \tag{16.2}$$

$$jk = -kj = i \tag{16.3}$$

$$ki = -ik = j \tag{16.4}$$

The quaternion vector,

$$\boldsymbol{q} = q_1\hat{\imath} + q_2\hat{\jmath} + q_3\hat{k} + q_4 \tag{17}$$

is made of magnitudes, q_{1-3}, in the original reference frame, and a scalar value, q_4. Curtis developed equations to find the quaternion vector with a known rotation around a given axis. The equations are presented in Eqs. (18.1-18.4):

$$q_1 = l \sin\left(\frac{\theta}{2}\right) \tag{18.1}$$

$$q_2 = m \sin\left(\frac{\theta}{2}\right) \tag{18.2}$$

$$q_3 = n \sin\left(\frac{\theta}{2}\right) \tag{18.3}$$

$$q_4 = \cos\left(\frac{\theta}{2}\right) \tag{18.4}$$

where $l, m,$ and n are the unit vector, in the inertial frame, which describes the rotation axis. θ is the amount of rotation around that axis. If the unit quaternion is known, [5] shows that the values can be used in the transformation in Eq. (19),

$$[\boldsymbol{Q_{Xx}}] = \begin{bmatrix} {q_1}^2 - {q_2}^2 - {q_3}^2 + {q_4}^2 & 2(q_1q_2 + q_3q_4) & 2(q_1q_3 - q_2q_4) \\ 2(q_1q_2 - q_3q_4) & -{q_1}^2 + {q_2}^2 - {q_3}^2 + {q_4}^2 & 2(q_2q_3 + q_1q_4) \\ 2(q_1q_3 + q_2q_4) & 2(q_2q_3 - q_1q_4) & -{q_1}^2 - {q_2}^2 + {q_3}^2 + {q_4}^2 \end{bmatrix} \quad (19)$$

This transformation can be used in the same way that the direction cosign matrix of Euler angles is used.

The power of quaternions can be seen when tracking the time rate change of the body frame. [13] shows that the time derivative of a quaternion can be modeled as a matrix that is based on rotation rates of the body,

$$\dot{\boldsymbol{q}} = \frac{1}{2}\begin{bmatrix} 0 & \omega_z & -\omega_y & \omega_x \\ -\omega_z & 0 & \omega_x & \omega_y \\ \omega_y & -\omega_x & 0 & \omega_z \\ -\omega_x & -\omega_y & -\omega_z & 0 \end{bmatrix}\boldsymbol{q} \quad (20)$$

where $\omega_x, \omega_y,$ and ω_z are the rotation rates of the body frame $x, y,$ and z axes. It should be noted that numerical integration can be used update the quaternion over time as the system dynamically evolves. It should be clear that the time derivative of the quaternion does not require Euler rate equations to find new body frame transformations, which means singularities are not a concern when rotating the precession axis through 90°.

While quaternions are not used in the following analysis, they are instrumental to the process of developing a robust attitude system and are recorded here for their potential use in a future robust attitude determination system.

F. Momentum

Newton's first law states: "Every body continues in its state of rest or of uniform motion in a straight line unless it is compelled to change that state by forces impressed upon it," [19]. Colloquially, this can be interpreted as "Objects in motion will stay in motion," which is a statement of momentum. Just as a moving train car has linear

momentum, which tends to maintain its motion down its tracks, a rotating body has a quantifiable tendency to continue rotating. This phenomenon is known as angular momentum. Controlling the magnitude and direction of a body's angular momentum is of the utmost importance.

When forces act on a body, the body will tend to move in response to the forces. Forces acting on the center of mass of a body cause the body to accelerate linearly. When forces act on a body along an axis that does not pass through the body's center, the forces create moments imparting rotational accelerations around the center of mass of said body. Rotational accelerations cause the body to rotate over time. Moments acting on a body can be considered with respect to some significant point, $\boldsymbol{P}$. The location of $\boldsymbol{P}$ can be chosen to represent some significant phenomenon, which is sometimes chosen as the center of mass of a planet or a component on a satellite.

The sum of all moments about $\boldsymbol{P}$ can be found by integrating the entire body's mass over the cross product of the distance of each particle of the body's mass to point $\boldsymbol{P}$ and their accelerations relative to the inertial frame [5], expressed in Eq. (21):

$$\boldsymbol{M_{p,net}} = \int \boldsymbol{r} \times \ddot{\boldsymbol{R}}\, dm \tag{21}$$

where $\boldsymbol{r}$ is the distance of an infinitesimally small mass element to $\boldsymbol{P}$ and $\ddot{\boldsymbol{R}}$ is the acceleration of that mass element with respect to the inertial frame origin [5]. Using the product rule from calculus, the moment about $\boldsymbol{P}$, Eq. (21), can be reorganized into Eq. (22),

$$\boldsymbol{M_{p,net}} = \frac{d}{dt}\int \boldsymbol{r} \times \dot{\boldsymbol{R}}\, dm + \dot{\boldsymbol{R}}_{\boldsymbol{p0}} \int \dot{\boldsymbol{R}}\, dm \tag{22}$$

$\dot{\boldsymbol{R}}_{\boldsymbol{p}}$ is the velocity of $\boldsymbol{P}$ in inertial space and $\dot{\boldsymbol{R}}$ is velocity of the mass element with respect to the inertial frame origin. The first term in Eq. (22) is known as the angular momentum of the body with respect to $\boldsymbol{P}$, as shown in Eq. (23),

$$\boldsymbol{H}_p = \int \boldsymbol{r} \times \dot{\boldsymbol{R}}\, dm \tag{23}$$

Choosing $\boldsymbol{P}$ as the center of mass of the spacecraft, and assuming that the velocity of $\boldsymbol{P}$ is small over time, $\boldsymbol{P}$ can be modeled as stationary and moments acting on the center of the spacecraft becomes Eq. (24),

$$\boldsymbol{M}_{\boldsymbol{Earth,net}} = \frac{d}{dt}\int \boldsymbol{r} \times \boldsymbol{v}\, dm + \boldsymbol{r} \times m\boldsymbol{a} \tag{24}$$

where $\boldsymbol{r}$, $\boldsymbol{v}$, and $\boldsymbol{a}$ become the distance, velocity, acceleration of center of Earth to the mass element [5]. Substituting the above two equations gives the time rate change of the angular momentum of the body in response to moments.

If the acceleration of the spacecraft around Earth is assumed to be small, then the moment equation about the spacecraft center of mass becomes Eq. (25),

$$\sum \boldsymbol{M}_{\boldsymbol{body}} = \Delta \boldsymbol{h}_{\boldsymbol{ECI}} \tag{25}$$

It should be noted that if no moments are exerted onto the spacecraft, its momentum is unchanged and therefore conserved.

G. Moment of Inertia

The moment of inertia is the measurement of a volumetric body's resistance to changes in orientation [5]. As previously explained, due to the governing laws of dynamics, any force applied to a body (anywhere other than toward or away from its center of mass) will create a tendency to rotate. The change in speed of an object's

rotation is directly related to the object's concentration of mass, its inertia. By definition, the relationship between a massive body's momentum and rotation in inertial space is:

$$\boldsymbol{h_X = I\omega_X} \tag{26}$$

Equation 26 is a reorganization of the equation of a rigid body's angular momentum. This relates the location of a portion of mass from the center of a body, $\boldsymbol{r_i}$, and its rotational velocity, as shown in Eq. (27)

$$\boldsymbol{h} = \int \boldsymbol{r_i} \times (\boldsymbol{\omega} \times \boldsymbol{r_i}) dm \tag{27}$$

Taking cross products of Eq. (27) and collecting them into their independent elements gives the large inertial tensor that can be found in Eq. (28),

$$\boldsymbol{I} = \begin{bmatrix} \int (y^2 + z^2)\, dm & -\int xy\, dm & -\int xz\, dm \\ -\int yx\, dm & \int (x^2 + z^2) dm & -\int yz\, dm \\ -\int zx\, dm & -\int zy\, dm & \int (x^2 + y^2) dm \end{bmatrix} \tag{28}$$

Each integral is an integration over mass and neglected for clarity. It can be noted that I_{xy} and I_{yx}, I_{xz} and I_{zx}, and I_{yz} and I_{zy} are called the products of inertia. Each set is mathematically identical, so the inertial tensor can be defined with only 6 unique elements. The matrix form of inertia will allow for convenient reorganization and decoupling of equations in the body frame as will be seen in the next section.

In most cases, the integration of a system will be carried out in such a way as to cancel and negate products of inertia to simplify dynamics.

H. Euler's Moment Equations

By taking the resulting equations from sections VII: G and VII: H and applying the fundamental equation of kinematics (Eq. (1)), a useful property can be expressed in a

convenient frame. The Euler Moment Equations show how the body of the spacecraft is affected when a moment is applied to it, as shown in Eq. (29),

$$\boldsymbol{M} = \dot{\boldsymbol{h}}_{\boldsymbol{ECI}} = \dot{\boldsymbol{h}}_{\boldsymbol{body}} + \boldsymbol{\omega}_{\boldsymbol{Body}} \times \boldsymbol{h}_{\boldsymbol{body}} \tag{29}$$

This equation is known as Euler's Moment Equation in vector form. Clearly, it can be seen that when a moment is exerted on a spacecraft, its momentum is changed.

If the body is assumed to be rigid, then its angular velocity will change in response to the changing momentum, as shown by [13]. Because $\boldsymbol{h}$ can be expressed in terms of inertia and angular velocity, the equations can further be reduced to;

$$\boldsymbol{M} = \boldsymbol{I}\dot{\boldsymbol{\omega}} + \boldsymbol{\omega} \times \boldsymbol{I}\boldsymbol{\omega} \tag{30}$$

When Eq. (30) is applied along a body's principle moments of inertia, the products of Inertia become zero and the equation can be reduced to a set of three equations in the body frame's "x", "y", and "z" axis;

$$M_x = I_x\dot{\omega}_x + \omega_y\omega_z(I_z - I_y) \tag{31.1}$$

$$M_y = I_y\dot{\omega}_y + \omega_x\omega_z(I_x - I_z) \tag{31.2}$$

$$M_z = I_z\dot{\omega}_z + \omega_x\omega_y(I_y - I_x) \tag{31.3}$$

Taking Euler's Moment Equation in the Z-body axis direction, Eq. (31.3), certain linearizing assumptions can be made [13]. For example, in the roll stabilizing controller to be developed, it is assumed that the system is passively stabilized in the "x" and "y" directions such that $\dot{\omega}_x$ and $\dot{\omega}_y$ are nearly 0 or that Iy and Ix are nearly identical. This assumption decouples the Z-axis from the other two when the second term goes to zero and the motion of the "z" axis is reduced to the simple, first order equation:

$$M_z = I_z\dot{\omega}_z \tag{32}$$

I. Equations of Motion

Euler's Moment Equations are the basis for describing the motion of a spacecraft [13]. The moments on a spacecraft can be separated into two categories, either controlling moments, such as ADCS thrusters, or disturbing moments, such as solar pressure. These moments are conventionally referred to as torques, T_c and T_d respectively.

If internal momentum exchange devices, such as reaction wheels are used, then their momentum can also be expressed independently of the body. Where h_b and ω_b refer to the body of the spacecraft and h_w refers to the wheel momentum [13]. Euler's Moment Equations become:

$$T_{cx} + T_{dx} = \dot{h}_{bx} + \dot{h}_{wx} + \left(\omega_{by}h_{bz} - \omega_{bz}h_{by}\right) + \left(\omega_{by}h_{wz} - \omega_{bz}h_{wy}\right) \quad (33.1)$$

$$T_{cy} + T_{dy} = \dot{h}_{by} + \dot{h}_{wy} + \left(\omega_{bz}h_{bx} - \omega_{bx}h_{bz}\right) + \left(\omega_{bz}h_{wx} - \omega_{bx}h_{wz}\right) \quad (33.2)$$

$$T_{cz} + T_{dz} = \dot{h}_{bz} + \dot{h}_{wz} + \left(\omega_{bx}h_{by} - \omega_{yz}h_{bx}\right) + \left(\omega_{bx}h_{wy} - \omega_{by}h_{wx}\right) \quad (33.3)$$

For the design of this controller, the "x" and "y" axis are passively stabilized and are neglected.

The controller designed in this paper will only actively control the "z" axis with a reaction wheel. Again, if the rotation rates of the x- and y- axis are assumed to be small, Eq. (33.3), the equation of motion in the z- direction reduces to Eq. (34),

$$T_{cz} + T_{dz} = \dot{h}_{bz} + \dot{h}_{wz} \quad (34)$$

One can clearly see that in a disturbance-free environment without external control torques, the left hand side of the equation goes to zero and becomes a statement of the conservation of momentum. Without disturbances or control torques, the change in

momentum of the spacecraft is equal and opposite the change in momentum of the reaction wheel.

A more useful interpretation of the equation of motion can be found by substituting the linearized Euler Moment Equation, Eq. (32), into the equation of motion around the z-body axis, Eq. (34) to result in the relation between torques and rotation rates of the body and wheel,

$$T_{cz} + T_{dz} = I_{bz}\omega_{bx} + I_{wz}\omega_{wx} \tag{35}$$

In Eq. (35), the sum of control and disturbance torques becomes directly related to the rotation rate of the spacecraft and wheel. It bears repeating that this linear equation relies on the assumption that the rotation rates in the "x" and "y" directions remain small or that the inertias in the "x" and "y" directions are similar and that all products of inertia are sufficiently close to zero.

As discussed previously, magnetic moments can be used to exert a controlled torque on the spacecraft. Unlike reaction wheels, magnetorquers can change the overall momentum of the spacecraft. Magnetorquers can be used to dump momentum accumulated from disturbances. The magnetic torque of a magnetorquer in a magnetic field can be expressed as:

$$\boldsymbol{T_B} = \boldsymbol{M} \times \boldsymbol{B} \tag{36}$$

where $\boldsymbol{M}$ is the vector of magnetic moments on the spacecraft in the body frame and $\boldsymbol{B}$ is the magnetic field that interacts with the spacecraft in body frame components [13].

When used as an actuator, $\boldsymbol{T}_B$ is a controlling torque in all three body axes; the

resulting component in the "z" axis can be expressed by combining Eq. (36) and Eq. (35). For control about the "z" axis, the resulting magnetic moment becomes Eq. (37),

$$T_{dz} = I_{bz}\omega_{bx} + I_{wz}\omega_{wx} - M_{bx}B_{by} + M_{by}B_{bx} \quad (37)$$

Equation (37) relates the spacecraft's rotation rates to the magnetic control moments, M_{bx} and M_{by}, and external disturbances, T_{dz}.

J. Disturbance Environment

1. Aerodynamic Torque

Aerodynamic torque is the consequence of moving a body near a planet's atmosphere. While the momentum transfer of atmospheric molecules on a spacecraft's surface is tiny, over time the momentum builds up and is a major concern for spacecraft in low Earth orbits. When non-symmetric surface areas around the centers of mass are affected by atmospheric drag, torques are developed on the spacecraft. In their text, *Spacecraft Environment Interactions,* Hastings and Garrett explain that momentum is added to the spacecraft from neutral gas molecules in the atmosphere; it is a key parameter limiting spacecraft lifetime and momentum wheel limits [20]. It is noted by [20] that deployable solar arrays can be a particular problem because they may track the sun in such a way as to present large surface areas to the oncoming atmosphere. [20] goes on to report that the ISS uses between 454 kg and 4536 kg of fuel every year to combat the effects of drag. As can be seen through some analysis, the effect will be somewhat attenuated for this CubeSat design.

Larson and Wertz present the equation for aerodynamic torque in their text as an interaction of the LEO environment and spacecraft geometry [4]. The aerodynamic torque acting on a spacecraft is:

$$\boldsymbol{T_{AD}} = \frac{1}{2}\rho \boldsymbol{V}^2 C_d A_s \left(\widehat{\boldsymbol{u_V}} \times \boldsymbol{s_{cp}}\right) \tag{38}$$

where ρ is the atmospheric density at the spacecraft's altitude, which can be approximated as 2e-11 kg/m^3 at around 400 km altitude. $\boldsymbol{V^2}$ is the square of the velocity. [5] calculated that velocity of a circular orbit at 400 km altitude is 7.68 km/s. C_d is the coefficient of drag and difficult to estimate exactly in the rarified air, [4] suggests that 2.25 is a realistic approximation. A_s is the spacecraft's surface area projected in the direction of travel; for the CubeSat traveling constantly in the negative z-direction, the cube's surface area is approximately 0.01 m^2. The cross product of $\widehat{\boldsymbol{u_v}}$, the direction of travel in the body frame, and s_{cp}, the distance vector between the center of mass and center of pressure, is the part of the equation that accounts for the offset of forces working on the spacecraft and separates the magnitude of the force into the proper axes.

It is precisely the aerodynamic forces which keep the TechEdSat stabilized in its "x" and "y" body frame directions. The center of pressure is placed far behind the center of mass of the CubeSat and allows the aerodynamic forces to align the center of pressure with the mass. One can visualize this as a badminton shuttlecock aligning itself with its velocity vector after being struck. Because the direction of travel can be approximated as directly in the negative z- axis, the cross product could be expected to go to zero and the aerodynamic torque can be assumed to be non-existent.

The worst-case scenario was defined as having a spacecraft with an angle of velocity offset of 1°/360° and an offset between the centers of mass and pressure is 20% of the width of the CubeSat. The cross product of the disturbances can be written as

$$\delta\left(\widehat{\boldsymbol{u_V}} \times \boldsymbol{s_{cp}}\right) = \begin{bmatrix} I & J & K \\ \delta\hat{V}_x & \delta\hat{V}_y & 1 \\ \delta\left(C_{px} - C_{mx}\right) & \delta\left(C_{py} - C_{my}\right) & \delta\left(C_{pz} - C_{mz}\right) \end{bmatrix} \tag{39}$$

where δ represents the slight disturbance of ideal conditions. In the "z" direction, the worst case scenario is taken in such a way that the perturbation effects are added to the cross product. The cross product in the "z" axis can be simplified to

$$\delta\left(u_V \times s_{cp}\right)_z = 2 * \ \delta\hat{V}_x * \ \delta\left(C_{px} - C_{mx}\right) \tag{40}$$

It is assumed that contributions in the "x" and "y" axes are of similar magnitudes and added together. For the disturbed conditions stated above, the worst-case cross product is 1.1e-4 m. Substituting this distance into the torque equation for the parameters listed above, the aerodynamic torque on a CubeSat under slightly perturbed conditions becomes:

$$T_{ADz} = \rho {V_z}^2 C_d A_s \left(\delta\hat{V}_x * \ \delta\left(C_{px} - C_{mx}\right)\right) \tag{41}$$

which is approximately 1.5e-9 N·m. Because the exo-brake causes the spacecraft to maintain its orientation with respect to the velocity vector, the aerodynamic torque is a secular disturbance.

2. Gravity Gradient Torque

As noted previously, gravity exerts a torque on the spacecraft and can be used to stabilize the craft if favorable conditions exist. When those conditions are not favorable,

gravitational torque is an appreciable disturbance that the control system must compensate for. [21] states that several missions have lost mission performance or failed because of disregard for gravitational torqueing. [4, 21] express the gravitational disturbance torque in a circular orbit as

$$\boldsymbol{T_{GD}} = \frac{3\mu}{{R_0}^3}\left(\hat{\boldsymbol{u}}_{\boldsymbol{e}} \times \boldsymbol{I_{body}} \cdot \hat{\boldsymbol{u}}_{\boldsymbol{e}}\right) \tag{42}$$

Here, μ is the standard gravitational parameter of Earth, taken to be 3.986e14 m^3/s^2. R_0 is the distance of the spacecraft from the center of Earth in meters; at an altitude of 400 km, R_0 is taken as 6.778e6 m. Also, $\hat{\boldsymbol{u}}_{\boldsymbol{e}}$ is the nadir direction in the spacecraft body frame. Since the positive "x" face is nominally oriented to be pointing toward Earth's surface, the unit vector is taken as $\{1, 0, 0\}^T$.

[21] lays out a general procedure for the compensation of gravitational torques. Initially, the worst case expected torque should be computed and then more careful analysis should be made if "… the analysis indicates that the gravitational torque is of consequence in the design." [21] goes on to recommend the use of principle axes and variation on spacecraft nominal orientation as significant torque parameters. Therefore, slight perturbations in pointing angle and inertia shall be considered in the expected torque from gravity gradient.

For spacecraft with body-frame-aligned principle inertial axes, [21] simplifies the torque of Eq. (42) into a maximum expected torque by comparing the largest and smallest principle moments of inertia,

$$T_{GD(\max)} = \frac{3\mu}{2{R_0}^3}(I_{max} - I_{min}) \tag{43}$$

Though this would provide an upper bound on gravitational torque, it neglects the fact that the spacecraft is passively stabilized and the effect on the "z" axis is of interest to the spin design. The TechEdSat's "z" axis is the axis of largest inertia, but due to linear algebra, the inertia of the "z" axis cannot affect gravitational torques in the "z" axis direction. Therefore, taking Eq. (43) as the disturbance torque due to gravity on the "z" body axis would grossly overestimate gravity's effects.

Instead, the roll axis equation presented later in [21] is used. Equation (44) calculates the gravitational torque in the roll axis for an Earth oriented spacecraft,

$$T_{GDz} = -\frac{3\mu}{2{R_0}^3}\left(I_x - I_y\right)\sin(2\psi) \tag{44}$$

The initial design anticipates inertial components in the "x" and "y" axis to be identical. This would negate any gravity contribution to the disturbance environment, so a 5% variation in the principle inertia about the "x" and "y" axes is assumed. Nominal spin angle, ψ, of 0^o would also zero out gravitational torques, so a worst case constant offset $\psi=1^0$ is added.

Taking the perturbations into the gravitational torque equation, Eq. (44) becomes

$$T_{GDz} = -\frac{3\mu}{2{R_0}^3}(0.05 * I_x)\sin(2 * \delta\psi) \tag{45}$$

The resulting force due to gravity disturbance torque on the "z" axis is approximately 8.3e-10 N·m. Again, because the spacecraft maintains its orientation with respect to the gravity gradient, the disturbance acts as a secular accumulation. This is a second order effect when comparing the torque to magnetic torque developed later this section; therefore, off-nominal orientation does not need to be modeled. It is assumed that the gravity gradient torque will remain the same, regardless of the spin angle orientation.

3. Solar Pressure Torque

High energy solar particles constantly bombard the satellite when in view of the sun. Though this is necessary for power generation in solar cells, the light also imparts momentum to the satellite that must be considered in disturbance calculations. [4] presents a worst-case solar pressure as Eq. (46),

$$T_{SD} = \frac{F_S}{c}\left(C_{sp} - C_g\right)\hat{A}_s\left(1 + q_{rf}\right)\cos I_s \tag{46}$$

The difference between C_{sp}, the center of solar pressure, and C_g, the center of gravity, is the moment arm of the force of sunlight, known as solar pressure; as a design margin, this difference is taken to be 20% the width of the CubeSat. F_s is the solar constant at Earth, taken as 1367 W/m^2 [4]. A_s is the area illuminated by the sun; this is assumed to be held constant and is set to 0.03 m^2, the largest surface area of the cube. The reflectance factor is q_{rf}; Larson and Wertz suggest a design value of 0.6 as a good assumption [4]. The speed of light, c, is 3.0e8 m/s. Because the period of spacecraft orbit is short compared to period of a solar orbit, the sun can be modeled as a fixed point over the course of an orbit and the disturbance can be assumed to be a cyclical response with the frequency of 1 orbit, about 90 minutes. I_s is the cyclic incidence angle of sunlight on the satellite and is approximated by a time varying function, Eq. (47),

$$I_s = \theta_{Smin} + (\theta_{Smax} - \theta_{Smin})\cos\left(\frac{t}{\tau_R}\right) \tag{47}$$

θ_{Smin}, 28°, is the difference between the spacecraft inclination and the angel between the sun and the inertia XY plane. θ_{Smax}, 75.1°, is the sum of the inclination and sun angle in opposition. Again, spacecraft inclination is taken to be the inclination of the ISS, 56.1°.

In ECI frame, the sun angle is taken to be the same as the Earth's axial tilt, 23°. The orbital period, τ_R, is taken to be 9400 sec. These values are a function of the worst-case angles between the sun, Earth, and the inclination of the spacecraft and oscillates between the minimum and maximum over a spacecraft's orbit. Although the incidence angle is only actually these values when the spacecraft and sun are in opposition, all other potential orientations have a smaller inclination thus this worst-case scenario is appropriate for first-order approximation of disturbances.

Equations (46) and (47) are combined to calculate the worst-case solar pressure torque of 3.8e-9 N·m and a minimum torque of 1.1e-9 N·m. This torque operates constantly on the spacecraft in the same direction over the entire orbit of the spacecraft and is seen to constantly add momentum to the spacecraft. Furthermore, it is assumed that the spacecraft is in constant view of the sun to slightly simplify the model; this means that the duration and location of eclipse are neglected. Though this slightly overemphasizes the overall torque generated by solar pressure, its magnitude is a sufficiently smaller than the magnetic dipole disturbances and is does not overly affect the spacecraft dynamics.

4. Magnetic Dipole Disturbance

When not utilizing the magnetorquer equations to de-spin the reaction wheel, it must be noted that the spacecraft still has some residual magnetic moment that will act as a constant source of disturbance. As the magnetic equation of motion has already been modeled, the response can be considered a disturbance that acts cyclically during the period of an orbit and has a magnitude dependent on the residual magnetic moment. [4]

suggests that an acceptable expectation for a small satellite's residual moment can be equivalent to 1 amp·m^2. Because a CubeSat is so much smaller than what Larson and Wertz were referring to as "small satellites," a value of 0.01 amp·m^2 was taken for analysis.‡‡ As derived in the magnetic moment control section, the magnetic field on the body can be expressed as a time varying vector that is a function of orbital phase. Looking at the harmonic nature of the magnetic field, in Fig. 8, it can be seen that the magnetic field of the "x" and "z" vectors average to zero over the course of a full orbit and that the magnetic field's y-axis introduces a constant, secular response.

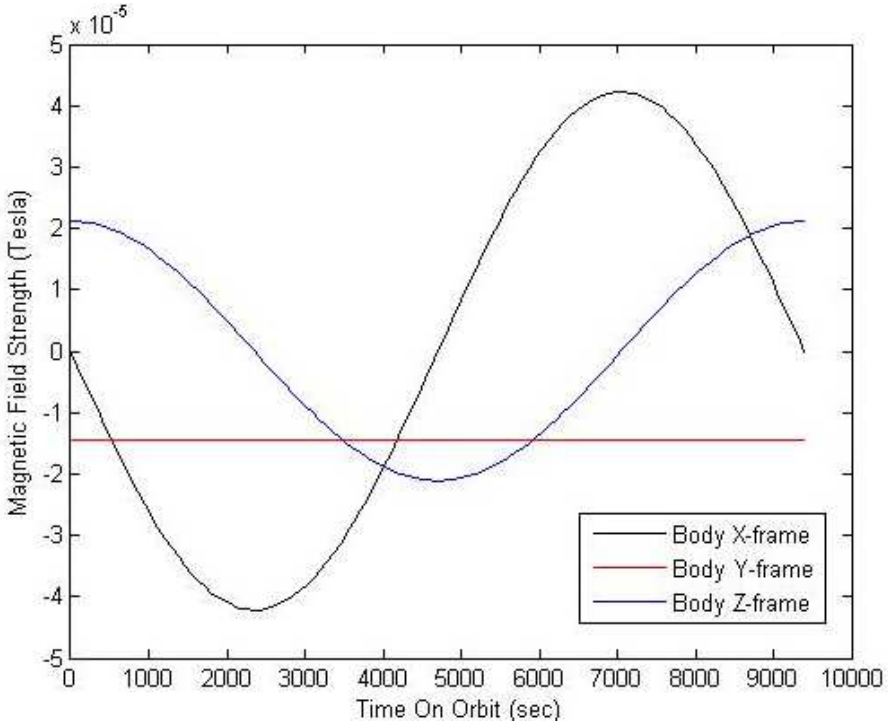

Fig. 8 Maximum magnetic field on body axis of spacecraft. Magnetic field magnitudes are expressed in the body frame and are calculated by holding the positive "x" face pointed nadir in 400 km orbital height at inclination of ISS.

‡‡ [4] consider their example spacecraft, FireSat, to be a "small" spacecraft weighing in at 140 kg. Later, they consider the early 5 kg Sputnik satellite to be a "small satellite." In a chart in their Design of Low-Cost Spacecraft section, they list masses of "small satellites" between 8.5 kg and 805 kg. [3] and others have since broken that range down into several size categories.

The magnetic disturbance can be simply considered a response of the spacecraft's residual moment to the y-component of the magnetic field. B_{by} is approximately -1.7e-5 Tesla. The magnetic disturbance in the z-direction can be stated simply as:

$$T_{Bd,secular} = B_{yd,nominal} M_x \tag{48.1}$$

$$T_{Bd,cyclical} = -B_{xd,nominal} M_y \tag{48.2}$$

Nominally, the spacecraft "z" body axis will face the "X_R" direction, the "x" body axis will face nadir, but the spin angle, ψ offsets the spacecraft by some appreciable amount. Transformation between the orbital reference frame and body frame can be expressed as:

$$\begin{Bmatrix} B_{bx} \\ B_{by} \\ B_{bz} \end{Bmatrix} = \frac{B_e}{{R_o}^3} \begin{bmatrix} 0 & -\sin\psi & \cos\psi \\ 0 & -\cos\psi & -\sin\psi \\ 1 & 0 & 0 \end{bmatrix} \begin{bmatrix} \cos\left(\varpi_R + \breve{\theta}_R - \eta_B\right)\sin\xi_R \\ \cos\xi_R \\ -2\left(\sin\left(\varpi_R + \breve{\theta}_R - \eta_R\right)\sin\xi_R\right) \end{bmatrix} \tag{49}$$

Taking these equations, the satellite will experience a worst-case magnitude of 1.7e-7 N·m. On orbit, the cyclic magnetic disturbance is modeled as a sin wave response with a magnitude of 4.2e-7 and a frequency of one orbital period (approximately one orbit every 9400 seconds). Because residual moment can be either negative or positive, the sign of these values is arbitrary at this point in the analysis.

5. Summary of Disturbances

The four major factors of external disturbance have been approximated and their magnitudes have been collected into Table 2. Cyclical disturbances are modeled as a sine wave with the frequency of one period while secular disturbances cause the spacecraft to accumulate momentum over time and are the reason that reaction wheels alone will not be a sufficient stabilization method. Assumptions are also collected into the table for ease of reference.

Table 2 Disturbances on spacecraft dynamics and list of their assumptions.

Name	**Mag. [N·m]**	**Secular / Cyclical**	**Assumptions**
Aerodynamic	3.7e-11	Secular	Circular orbit Center of Pressure and Mass misalignment of 20% the width of CubeSat Velocity vector misalignment of 1°
Gravity Gradient	8.4e-10	Secular	Magnitude "x" and "y" principle inertia 5% difference Velocity vector misalignment by 1°
Solar Pressure	4.3e-09	Secular	'q'=0.6 Worst-case incidence when sun and orbit are in opposition Center of pressure offset by 20% the width of CubeSat
Magnetic Dipole	4.2e-07 & 1.4e-07	Cyclical & Secular	Residual dipole assumed to be 0.01 amp·m^2 Magnetic field approximated as dipole Circular orbit with spacecraft in nominal orientation

VIII. Actuator Control Development

A. Euler Control Laws

Apart from modeling the motion of a body, it is important to define the theory of how to exert control. One commonly used method is called closed-loop feedback, where a desired response is compared to measured response and then the system is directed to act with a compensating force. The control law is the logic behind the actuating commands. For the spacecraft designed here, it is important to design a control law that sufficiently meets the needs of the mission without calling for the design of an unrealizable actuator.

The system should be able to control the spin rate and position of the spacecraft to some desired angle within the context of a standard orbit. Given a number of assumptions to be discussed later, the control law can be stated as the simple directives:

$$\omega_z \rightarrow \omega_{z,desired}\ as\ t\ \rightarrow\ \infty \tag{50.1}$$

$$\psi \rightarrow \psi_{desired}\ as\ t\ \rightarrow\ \infty \tag{50.2}$$

That is to say, the spacecraft's spin rate and the angular position are driven to some desired spin rate and position as elapsed time approaches infinity [22]. Levine notes that these are asymptotic conditions where existing values will get systematically closer to the desired value over time and that a rate of convergence should be chosen so that the desired state is reached in a satisfactorily short amount of time.

Standard operating procedure will be to hold the spacecraft at a desired position. An example might be to point the antenna or camera toward Earth. In this scenario, the spacecraft's position will match some desired position and its rotation rate will be forced to zero. The control strategy, Eqs. (50.1) and (50.2), become:

$$\psi \rightarrow \psi_{desired}\ as\ t\ \rightarrow\ \infty \tag{51.1}$$

$$\omega_z \rightarrow 0\ as\ t\ \rightarrow\ \infty \tag{51.2}$$

Negative feedback control can be used to drive the state of the spacecraft such that the error between the current state and desired state becomes small. The error signal equations are:

$$\psi_{desired} - \psi = \psi_{error} \tag{52.1}$$

$$0 - \omega_z = \omega_{z,error} \tag{52.2}$$

where $\omega_{desired}$ is 0 rad/sec. Taking the linearized equation of motion (without needing to model the interaction of reaction wheel control) and applying gains to the error signals the control law, Eqs. (52.1) and (52.2), as shown by [22], create the control effort equation, Eq. (53),

$$u_z = -K_{frame}(\psi_{error}) - K_{d,frame}\left(\omega_{z,error}\right) + I_{bz}\dot{\omega}_{bz} \tag{53}$$

Here K_{frame} and $K_{d,frame}$ represent constant gains that scale responses and I_{bz} and $\dot{\omega}_{bz}$ represent the spacecraft inertia and rotation rate in the controlled, "z" direction of the body frame. The goal of the control process is to exert a control authority, u_z, such that the errors signals become small. The closed loop equation can be expressed as:

$$I_{bz}\dot{\omega}_{bz} + K(\psi_{desired} - \psi) + K_d(\omega_z) = 0 \tag{54}$$

Figure 9 is the linear block diagram representation of this control law in negative feedback form [4]. When the error between the desired position and actual position is large, a large error signal is fed into the rotation rate control loop. The rate control loop then compares the large desired rotation rate to the actual rotation rate and acts to modify the rotation rate accordingly. As the actual position approaches the desired position, the signal sent to the rate loop becomes small and the spacecraft slows down. This process is iterated until the spacecraft has sufficiently reached the ideal pointing condition with zero velocity.

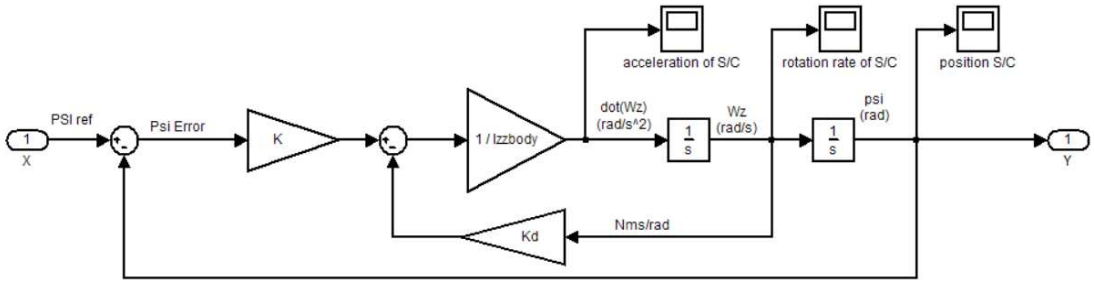

Fig. 9 Block diagram of the control law. Shown here is the implemented Simulink model for spin axis control.

Up to this point in the design, the reaction wheel dynamics are considered to provide an infinite amount of torque without limit and can do so instantaneously and without

error. The perfect actuator assumptions are sufficient to design an ideal response, but will be redressed once the wheel and disturbance models are developed later in this chapter. The spacecraft control law is a model that can be used to tune control gains and serves as a platform to develop a more complex system.

B. Reaction Wheel Design

As previously discussed, reaction wheels allow for the transfer of momentum inside a closed system. Rather than change the overall momentum of the system, a spinning wheel can "store" a portion of the spacecraft's momentum to allow for the precise control of the spacecraft spin. The wheel and motor exert an internal torque which acts on the spacecraft in an equal and opposite direction due to the conservation of momentum [13]. Referring back to the linearized equation of motion, Eq. (34), with no external control moments or disturbances on the "z" body axis, wheel dynamics on the body can be written as Eq. (55),

$$\dot{h}_{wz} = T_w = -\dot{h}_{bz} \tag{55}$$

where $\dot{h}_{wz}$ is the change in momentum of the wheel, T_w is the torque generated by the wheel, and $\dot{h}_{bz}$ is the change of the spacecraft's momentum in the "z" direction.

The reaction wheel is modeled as a torque generator and electronics package. The reaction wheel assembly is composed of a motor and rotary mass aligned to spin along the principle axis of the axis to be controlled. The torque output by a reaction wheel is the difference between the motor torque and the retarding friction torque of the wheel's axle. The motor is modeled simply as an electronics package and a gain, k_{motor}, that transforms current into a torque. Feedback control takes the form of a current monitor

that compares the intended motor current to the actual current input to the motor. The rotating components of the motor create an electromagnetic field that works against the motor and effectively creates a voltage drop that lowers the actual current being input to the motor. Because the system is limited to providing a certain amount of voltage and current, saturation limits are placed in the forward feed line of the wheel. Friction loss is modeled as Eq. (56),

$$T_f = b * \omega_{rel} \tag{56}$$

where b is the viscous friction coefficient of the motor, and ω_{rel} is the relative velocity between the wheel and spacecraft. Figure 10 shows the Simulink diagram of the reaction wheel design.

This reaction wheel diagram is useful for understanding the expected performance of a reaction wheel and allows for the tailoring of control gain, k_wheel. The transfer function of the system between the desired torque and generated torque can be seen in Eq. (57),

$$\frac{\dot{h}_w}{T_c} = \frac{\frac{k_{wheel}}{R_m s}\left(\frac{s}{s+b\left(\frac{1}{I_{wz}}+\frac{1}{I_{bz}}\right)}\right)}{1+\frac{k_{wheel}}{R_m s}\left(1+\frac{k_v k_m}{k_{wheel}}\left(\frac{1}{I_{wz}}+\frac{1}{I_{bz}}\right)\left(\frac{s}{s+b\left(\frac{1}{I_{wz}}+\frac{1}{I_{bz}}\right)}\right)\right)} \tag{57}$$

Here, k_{wheel} is the tunable control gain; R_m is the electrical resistance of the motor; I_{wz} and I_{bz} are the inertias of the wheel and body, respectively, along the "z" body direction; and b is the viscous friction. The lower fraction contains k_v, a gain that transforms wheel rotation rate into voltage drop due to back-EMF. Also, k_m is the motor gain is assumed to be a linear function that converts electrical current into torque.

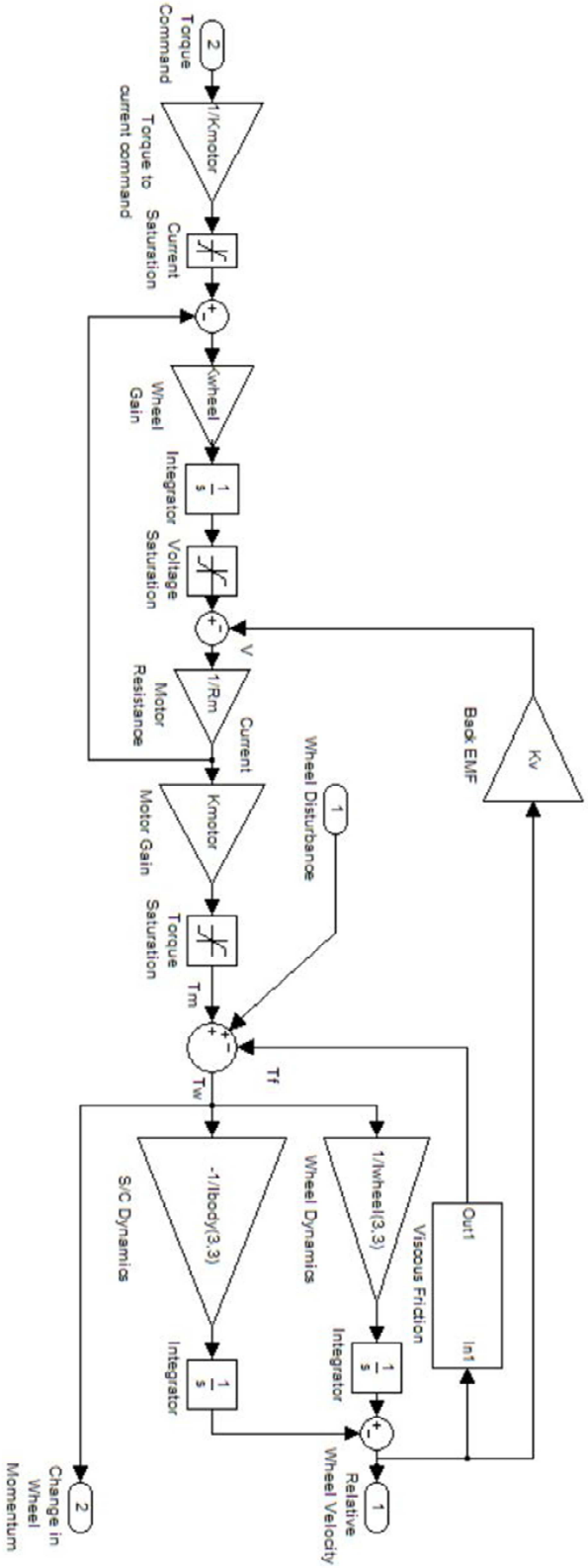

Fig. 10 Simulink model of simple reaction wheel.

C. Magnetorquer Design

Magnetorquers are simple coils of conducting wire. Electricity moving through the wire will create a magnetic moment. A magnetorquer can be used as an actuator by controlling the current in the coil to create a desired torque on the spacecraft body. This will be utilized to change the overall momentum of the spacecraft. If done in a controlled measure, they can be utilized to remove momentum from the reaction wheels without significantly altering the position of the spacecraft.

A basic control law, presented by [13], for unloading torque from reaction wheels can be expressed as:

$$\boldsymbol{T} = -K_{mag}(\boldsymbol{h_w} - \boldsymbol{h}_{desired}) = -K_{mag}\Delta\boldsymbol{h} \tag{58}$$

Here, $\boldsymbol{T}$ is the torque desired from the magnetorquer, K_{mag} is the scalar control gain, $\boldsymbol{h_w}$ is the reaction wheel torque and $\boldsymbol{h}_{desired}$ is the desired momentum remaining in the wheel after the maneuver. The gain K_{mag} should be chosen based on the characteristics of the magnetorquer and the desired rate of momentum removal.

For the one degree of control ADCS, this can be expressed purely in the z-axis direction. Utilizing the magnetorquer and control equations, the control problem is:

$$-K_{mag}\Delta\boldsymbol{h} = \boldsymbol{M} \times \boldsymbol{B} \tag{59}$$

Here, $\boldsymbol{M}$ is the control moment applied and $\boldsymbol{B}$ is the magnitude of the magnetic field in the spacecraft body frame at the spacecraft's position. Unfortunately, [13] states that the cross product of $\boldsymbol{M}$ and $\boldsymbol{B}$ result in a singular 3 by 3 matrix that cannot be inverted. It would be desirable to find the moment required to render the desired momentum rejection from the system.

[13] suggests that using the assumption that the magnetorquers are only used when their magnetic moments are perpendicular to the magnetic field will allow Eq. (59) to be pre-multiplied by $\boldsymbol{B}$ and result in a triple cross product that can be simplified to a grouped dot product with the bonus of a portion canceling due to the perpendicular vectors, as seen below:

$$\boldsymbol{B} \times -K_{mag}\Delta\boldsymbol{h} = \boldsymbol{B} \times \boldsymbol{M} \times \boldsymbol{B} = B^2\boldsymbol{M} - \boldsymbol{B}(\boldsymbol{M} \cdot \boldsymbol{B}) \tag{60}$$

$$\frac{-K_{mag}(\boldsymbol{B}\times\Delta\boldsymbol{h})}{|\boldsymbol{B}|^2} = \boldsymbol{M} - \boldsymbol{0} \tag{61}$$

The magnitude of the magnetic field on orbit can be approximated by the function:

$$B = |\boldsymbol{B}| = \frac{B_e}{{R_0}^3}\sqrt{1 + 3\sin^2\lambda_B} \tag{62}$$

In Eq. (62) B_e is Earth's magnetic dipole strength in Tesla·m^3 and R_0 is the distance from the center of Earth to the satellite in m, and λ_B is the angle between the satellite's inclination and the plane perpendicular to the magnetic dipole axis. Earth's magnetic dipole is 7.96e15 Tesla·m^3 [13]. Since the ISS is the expected launch platform, an inclination of 51.6^o is chosen for the spacecraft; recent magnetic maps put the magnetic pole at around 86^o north [18]. As the spacecraft's right ascension node marches around the planet, the worst case will give a λ_B of 47.6^o. At an altitude of roughly 400 km, the spacecraft will experience a magnetic field of 3.5e-5 Tesla.

When condensed to matrix form, the magnetic control equation, Eq. (61) can be written as:

$$\begin{bmatrix} M_x \\ M_y \\ M_z \end{bmatrix} = \frac{-K_{mag}}{|B|^2}\begin{bmatrix} B_y\Delta h_z - B_z\Delta h_y \\ B_y\Delta h_x - B_x\Delta h_z \\ B_x\Delta h_y - B_y\Delta h_x \end{bmatrix} \tag{63}$$

Here, the magnetic components are transformed into the body frame by the reference to body frame transformation developed in the kinematics section of the same name. Further assumptions are taken for the design of the stable-single axis reaction wheel system. Assuming that the spacecraft's momentum response in the "y" and "x" directions is slow, all momentum can be dumped from the "z" axis. Because the system is designed for one reaction wheel in the "z" direction of the body, moments can be applied about either the "x" or "y" direction. Control with the magnetorquer is applied by a single magnetorquer for ease of integration and power requirements. The axis should be chosen for ideal integration of magnetorquer hardware and the expected trajectory of the CubeSat. For this model, the "x" axis was chosen because of the constant magnitude of the magnetic field in the "y" body axis.

Reducing the reaction wheel speed to 10 rpm, or about 1 rad/s, serves to increase the fidelity of the model further by avoiding un-modeled dead-band dynamics (near 0 rpm) of the reaction wheel. The control moment equation, Eq. (63) becomes:

$$M_x = \frac{-K_{mag}}{|B|^2}\left(B_y(h_z - I_{zw}\omega_{LowerLimit})\right) \tag{64}$$

The control moment M_x is developed by a magnetorquer that must be sized appropriately so that the actuator does not become saturated. If simulations indicate that the magnetorquer becomes saturated, either a larger, more massive magnetorquer can be designed or performance can be scaled back by lowering the control gain, K_{mag}. [13] notes that the body is not constantly perpendicular to the magnetic field, and that the actual amount of torque on orbit will be somewhat less than anticipated by the approximation, but this provides a good first order approximation. It is worth noting that

$\boldsymbol{B}$ should be directly measured while on orbit and routinely updated with a magnetometer. Because the goal of the magnetorquer in this design is only to remove momentum, not exert fine control over attitude, this linearization should be sufficient.

With the desired control moment equation designed, the equation of motion for magnetic torque, Eq. (36), can be employed to find the overall torque created by the magnetorquer, Eq. (64). The magnetic control torque generated in the z-body frame is combined as:

$$T_{cB} = \frac{-K_{mag}}{|B|^2}\left(B_y{}^2(h_z - I_{zw}\omega_{LowerLimit})\right) \tag{65}$$

This equation assumes that the K_{mag} is generated by a magnetorquer oriented in the x-body axis. The implementation of the control torque can be seen in Fig 11.

Whatever K_{mag} is selected, it should have the property of removing the momentum from the system in a sufficiently quick amount of time, without requiring that the magnitude of the moment M_x created by the magnetorquer be larger than the magnetorquer could produce.

D. Friction Compensator

Due to the interaction of wheel friction and disturbances, it was found that the model will see some constant acceleration offset. Though this acceleration is small, it is sufficient enough to cause the system to diverge over time. Preliminary analysis showed that the spacecraft attitude drifted by 1° every 9 hours. Investigation resulted in a simple solution. Friction losses were found to cause the drift problem and needed to be compensated for by increasing the command torque by the exact amount of friction lost.

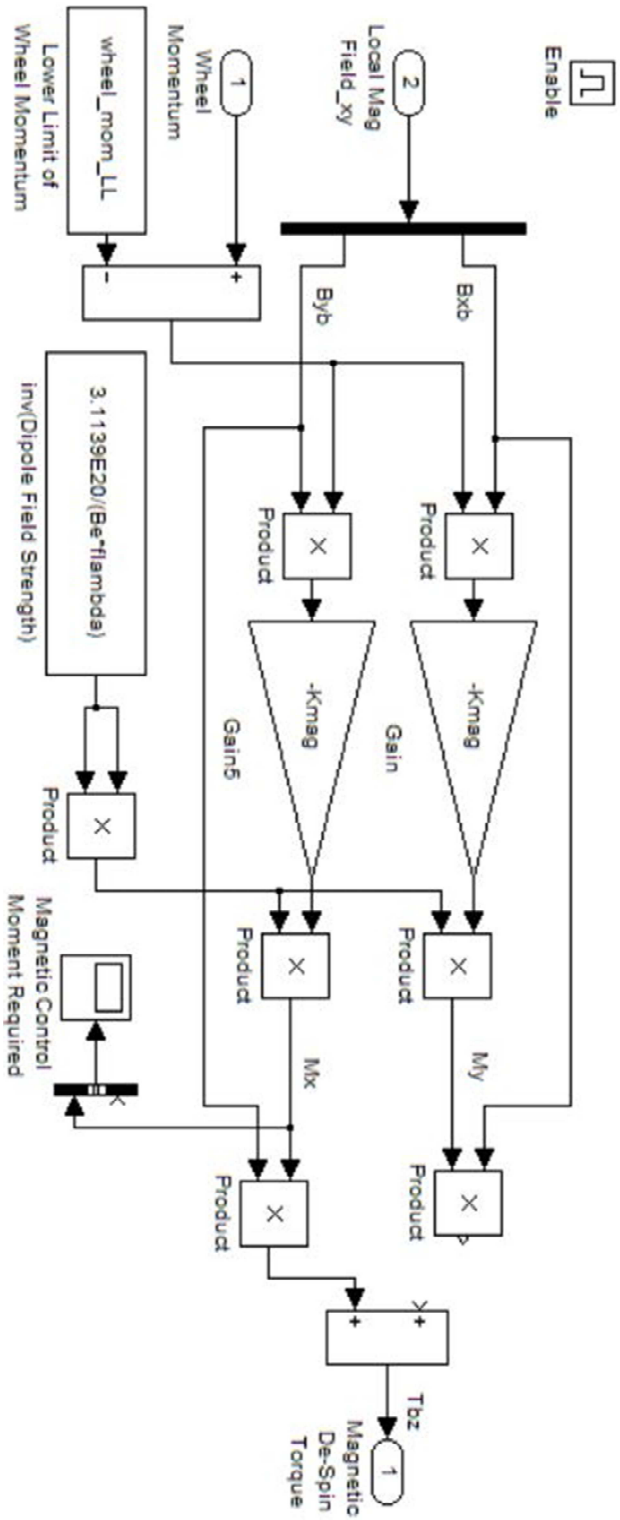

Fig. 11 Momentum dumping control loop. This block structure allows easy expansion for use about the "y" axis, current design utilizes only one x-axis magnetorquer.

In their publication, "Estimating Friction Parameters in Reaction Wheels for Attitude Control," [23] Carrara and Kuga introduced a control equation for their PID controller based on the addition of a friction compensator. Their modified controller took their PID controller design without a friction compensator and super imposed a dynamic friction compensator as a non-linear controller to account for their nonlinear friction losses. The friction model used in [23] accounted for viscous, coulomb, and Stribeck frictions. The model used here will be a linearized version of their model, accounting only for viscous friction:

$$i_{command} = \frac{T_{command}}{K_{motor}} + \frac{b}{K_{motor}} \omega_{rel} \tag{66}$$

The compensator applies a model of the expected friction force back to the command torque. The set-up can be seen in Fig. 12. The dotted outline shows the new addition of the modeled friction and torque to current conversion. This new signal is added in front of the gain saturation block because it is acting as a signal booster that could theoretically still saturate the current into the motor.

E. System Integration

The reaction wheel can be placed in its entirety into the control law to create a more realistic model and to observe the effects of disturbances on the vehicle. It is necessary to drive the wheel to create a torque in the negative sense of the direction of satellite's motion; therefore, a negative gain blocks have been added to the system to indicate this fact. The forces created by the reaction wheel act on the satellite's inertia and are controlled by the feedback compensators, seen in Fig. 13.

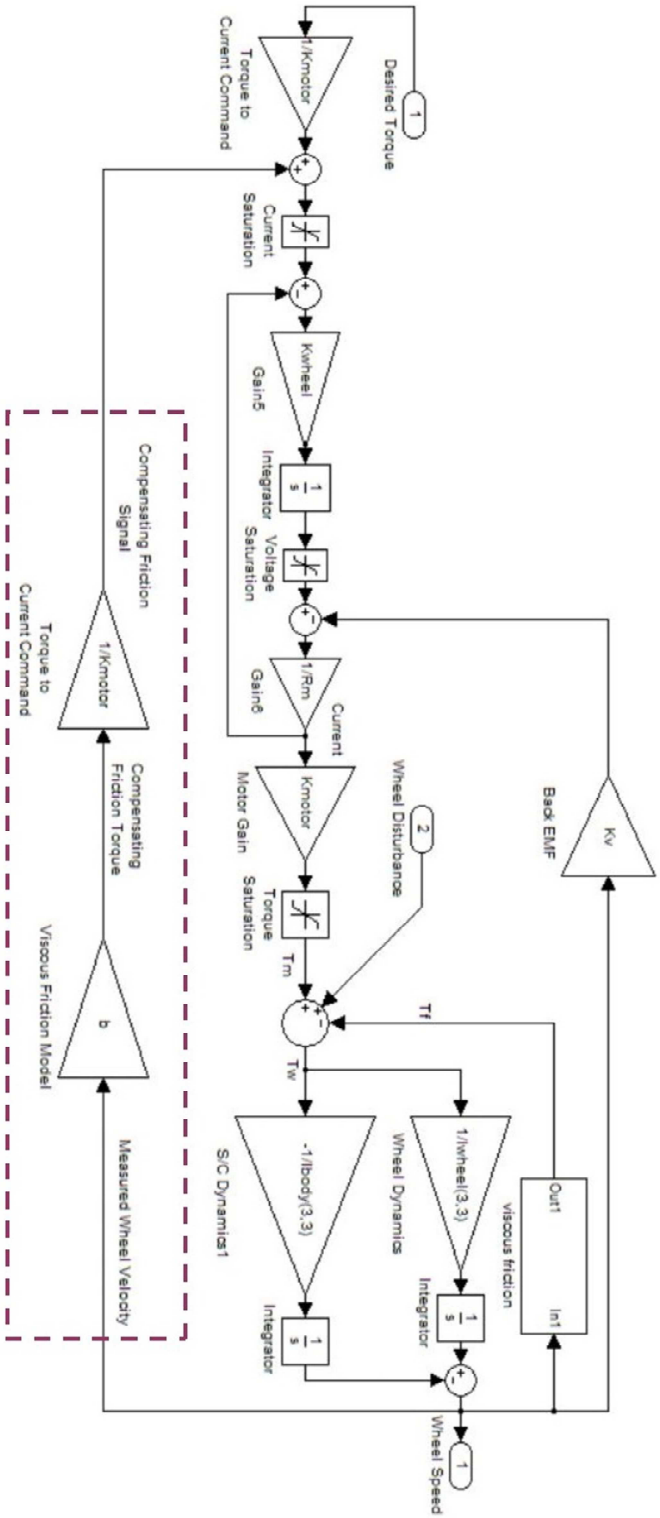

Fig. 12 Dynamic friction compensator to boost input signal. Addition of the compensator shown in dotted box.

The system responds to a signal to acquire a target position by engaging the reaction wheel. By creating a torque on the reaction wheel, the wheel's momentum changes. This forces the spacecraft's momentum to change by some known amount and enables the satellite to rotate toward its target. When external disturbance forces are applied to the spacecraft, they are accounted for as a signal added to the control torque exerted by the reaction wheel. The wheel assembly independently experiences noise and is modeled as a signal at the summation junction where friction losses and control torques are combined. Once some specified saturation limit is reached, the magnetorquer control loop automatically engages to remove the excess momentum from the wheels.

IX. Results and Analysis

A. Analysis of the Control Law

Since the equation of motion for the spin axis only needs the inertia of the body in the z-axis to relate spin rate to control effort, the only quantity of the spacecraft that needs to be defined is the inertia. Because this paper is a conservative design of a CubeSat, the chosen inertia is that of a completely solid block of aluminum in the shape of a 3U cube. The most important inertia in this analysis is that of the spin axis, $Iz = 4.90e-07$ kg·m^2. This moment of inertia will serve to give a realistic expectation of the performance that will be needed to sufficiently control the satellite. It is assumed that the deployed exo-brake will have very small effect on the overall inertia.

The gains K_{frame} and $K_{d,frame}$ are variables that are tuned to give the spacecraft the desirable responsiveness. To observe the effects of variation of the gains, the model can be condensed into a single transfer function through block manipulation.

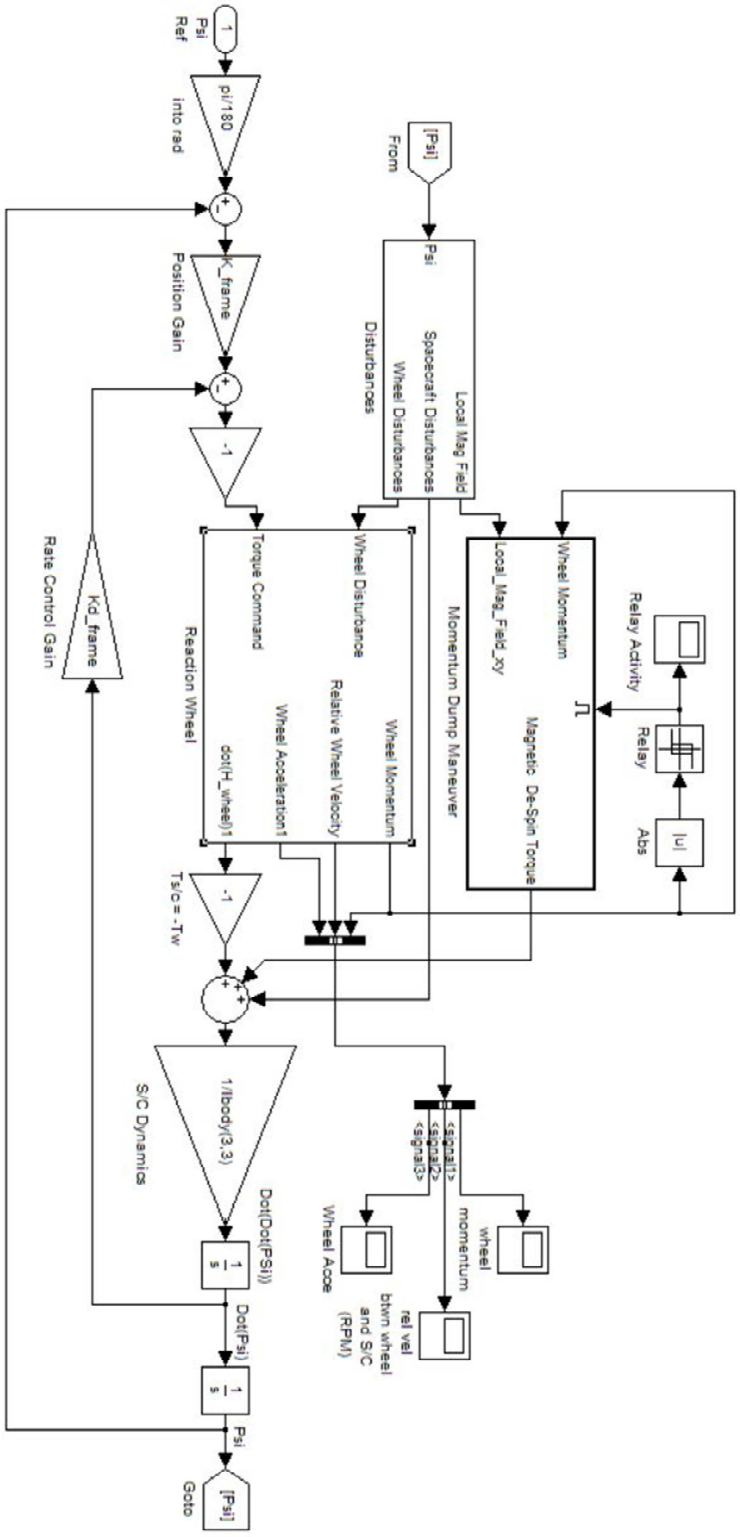

Fig. 13 Fully integrated control system with reaction wheel, disturbances, and control gains. Sufficiently saturated wheel activates momentum dumping maneuver.

Equation (67) is the control law transfer function:

$$\frac{\psi}{\psi_{desired}} = \frac{K_{frame}}{s^2 + \frac{K_{d,frame}}{I_{bz}} s + \frac{K_{frame}}{I_{bz}}} \tag{67}$$

Here, K_{frame} is the chosen system proportional gain, $K_{d,frame}$ is the derivative gain, and I_{bz} is the body's inertia around the spin axis.

Stability characteristics are determined by the denominator of the transfer function. Second order transfer functions are often modeled as mass spring systems whose response is well-known. The control law response will follow Eq. (67)'s characteristic equation,

$$s^2 + \frac{k_{d,frame}}{I_{bz}} s + \frac{K_{frame}}{I_{bz}} = 0 \tag{68}$$

This is conceptually identical to the familiar second order mass spring system,

$$s^2 + \frac{2\zeta\,\omega_0}{m} s + \frac{{\omega_0}^2}{m} = 0 \tag{69}$$

Here, m is the mass, ω_0 is the natural frequency, and ζ is the system damping ratio. The K_{frame} gain can be thought of as the intensity of the response to an error signal present in the loop while $K_{d,frame}$ contributes to the damped response of the system. This is a useful convention because the complexities of a spacecraft's control response can be abstracted to a simple, damped spring-mass. Relating these equations together, the natural frequency and damping of the spacecraft motion can be calculated by the following equations:

$$\omega_0 = \sqrt{\frac{K_{frame}}{I_{bz}}} \tag{70.1}$$

$$\zeta = \frac{K_{d,frame}}{2\sqrt{K_{frame} I_{bz}}} \tag{70.2}$$

Thus, K_{frame} will directly affect frequency response of the system and $K_{d,frame}$ can be chosen to create a desired damping response. Because it is desirable for the spacecraft to quickly arrive at its target with little to no overshoot, yet not respond too rigidly, a "damping ratio" of 0.75 was chosen as a design constraint. From this, an equation relating K and K_d was developed,

$$K_{d,frame} = 2\zeta\sqrt{K_{frame}I_{bz}} \tag{71}$$

Once an ideal ratio of the control gains has been determined, values for K and K_d can be chosen for an ideal crossover frequency as will be explained below. A Matlab script was used to sweep through values of K, given the ideal damping ratio to find a satisfactory frequency response to the system.

To show that a given system can sufficiently respond to disturbances and remain in stable equilibrium, phase and gain margins were found with the use of a Bode plot. By convention, systems should have a phase margin of at least 45^o and a gain margin of at least 6 dB. One benefit of the Bode plot is that it also charts the crossover frequency and directly relates to the bandwidth of a system. The crossover frequency is the frequency at which the transfer function first crosses the zero decibel mark. The bandwidth is defined as the frequency three decibels below the crossover frequency. It is critical to intelligently choose gains which desirably set the crossover frequency and bandwidth. A sufficiently low bandwidth will amplify control signals but reject high frequency noise. Space is vast and empty; most operations of spacecraft attitude control are pre-planned and are executed slowly, over long periods of time. The response time of the spacecraft should be slow enough to reject disturbances, but fast enough to meet the pointing goals

laid out in the design requirements. Crossover frequency between 1 rad/sec and 10 rad/sec should be sufficient to acquire a target, but low enough to reject noise.

Matlab was used to automatically generate Bode plot responses from broken loop Simulink model. The specific diagram used can be seen in Fig. 14. K_{frame} and $K_{d,frame}$ were varied until ideal crossover frequencies were found. 3 sets of gain variables were found using this strategy, which allows for a more robust understanding of the sub-system's flexibility of performance versus its bandwidth. Table 3 below, relates a given gain to performance criteria.

Table 3 Control law gain values.

Crossover Frequency (rad/s)	**K_ frame**	**Kd_ frame**	**Damp-ing Ratio**	**Band-width (rad/s)**	**Rise Time (s)**	**Settling Time (2%)**	**Phase Margin (deg)**	**Gain Margin**
1	0.0052	0.0126	0.75	1.37	1.34	8.0	67.7	Inf
5	0.129	0.0627	0.75	6.82	0.27	1.6	67.7	Inf
10	0.52	0.126	0.75	13.7	0.13	0.8	67.7	Inf

Taking these values for K and Kd into the Simulink block diagram, the system will respond to commands crisply. When commanded to rotate by one degree, the system converged in short order with virtually no steady-state error. When commanded to slew at 1°/sec, the system was able to do so with a slight steady state error. Because this CubeSat mission does not put large significance in overly rapid responses, a settling time of less than 10 seconds can be considered sufficient performance given the simplistic control law.

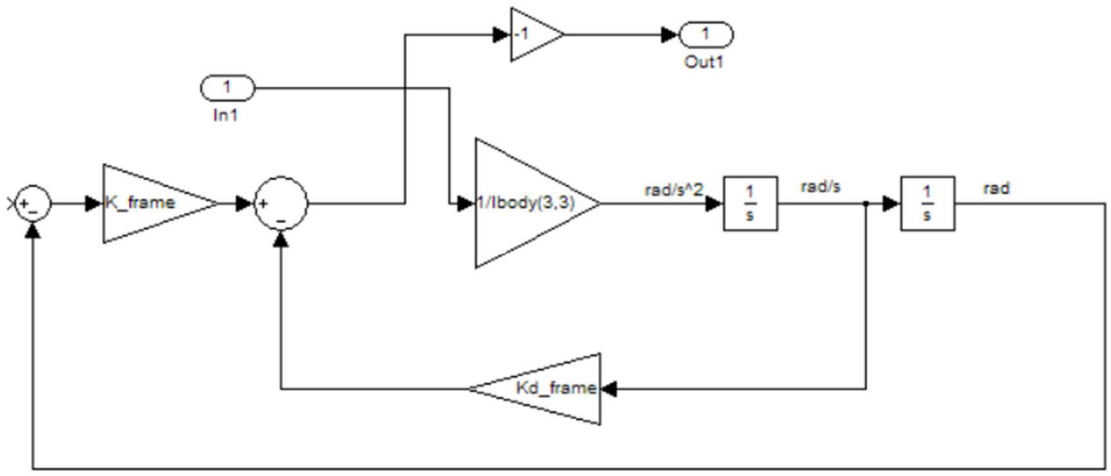

Fig. 14 Broken loop diagram for bode analysis of the control law.

B. Reaction Wheel Analysis

The design of the reaction wheel is constrained by system capabilities. The wheel must be small enough, low power enough, and efficient enough to operate inside a CubeSat. Assuming that the system will be controlled by an Intel Edison microprocessor, the system will be limited to 5 V and 2.5 Watts. The wheel must also fit into a CubeSat form factor. The TechEdSat team is willing to commit a full half of a U to pointing control, so the wheel, hardware and mounting equipment must fit into a 10 cm x 10 cm x 5 cm volume.[§§] A rough approximation of a CubeSat reaction wheel mass has been drafted in Creo Parametric and can be seen in Fig. 15. Its "z" axis-inertia of 5.897e-05 kg·m^2 shall be used in the design and is assumed to be close to the actual inertia of the final design.

[§§] Discussion with TechEdSat's Primary investigator, Marcus Murbach.

Motor properties are unique to each motor and because a specific motor has not been chosen for this design, a set of realistic motor parameters are used to represent what a reaction wheel motor could be like. Carrara and Kuga, [12] designed a speed and current control-loop control scheme for a Brazilian university's experimental reaction wheel control. [12]'s system was sized for a wheel inertia of 1.5e-3 kg·m^2. Even though the values come from a realized system, it would be unrealistic to apply them to a satellite roughly the size of their reaction wheel; therefore, values used in this paper will be scaled by the ratio of wheel inertias. The scaling ratio of 0.0393 was applied to Carrara and Kuga's motor gain, K_{motor}, and viscous friction.

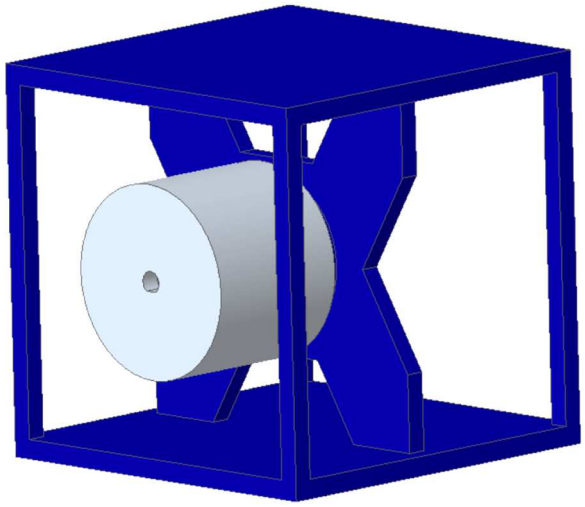

Fig. 15 Reaction wheel inside of mock CubeSat. Illustration shows relative size comparison of wheel to a single U of the CubeSat.

Motor gain is a linearization that directly and instantly converts the current fed to the motor into torque. Torque lost due to viscous friction is modeled. Viscous friction is assumed to be the only type of friction operating on the system and is modeled as a linear function of the wheel rotation rate. The maximum torque the system is capable of

producing is taken as the product of the maximum current and the scaled motor gain. The back-electromagnetic-force (BEMF), k_v, was taken from a micro motor with torque and voltage operating parameters similar to the operational voltage and motor gain.[***] Back EMF is modeled as a voltage loss that is proportional to the wheel rotation rate. It is assumed that the ideal motor resistance, which perfectly scales the voltage and current limit is a realistic value. Ohm's law is a famous equation that relates current to voltage by resistance and, as it applies to the motor, can be seen below,

$$V_m = i_m R_m \tag{72}$$

V_m is the voltage, i_m is the current, and R_m is the resistance. It should follow that the equation can be reorganized to calculate the ideal resistance that would compare maximum available current to voltage, and is taken to be 10 ohms. Although these values do not necessarily correspond to any motors on the market, it is held that these values are realistic for an appropriately sized system. Motor parameters have been collected in Table 4.

Table 4 Reaction wheel parameters.

K_{motor} [N·m/amp]	Motor Resistance, R_m [Ohm]	Viscous Friction, b [N·m·s]	Voltage Saturation [V]	Current Saturation [amp]	Max Torque [N·m]	Back EMF, k_v [V·s]
8.964e-4	10	1.899e-7	+/- 5	+/- 0.5	4.482e-4	1.00e-3

The reaction wheel can be tuned by adjusting the K_{wheel} gain value. Using Matlab's linearization software to see the broken loop response of Fig. 16, the system's frequency

[***] Pitman DC022C-1 brush DC motor, 6.0 V

response can be found. The Bode diagram, Fig. 17, verifies that the model is stable and acts as a first order system. It is seen to have infinite gain and phase margin of 90° and so will be sufficiently stable. An infinite gain margin means the wheel model will be stable for any desired K_{wheel}. Choosing a crossover frequency of 60 rad/second will ensure that the reaction wheel response is much faster than the control system response and thus will be able to resolve demands for momentum change as fast as the system develops them, as was assumed in the Euler control law development.

Unlike the control laws, a damping ratio cannot easily be set. Considering the values for the transfer function, simplifications can be made to better understand the dominant factors in the reaction wheel response. The viscous friction term and the inverse of spacecraft inertia are small, so the transfer function, Eq. (56), can be rewritten as:

$$\frac{\dot{h}_w}{T_c} = \frac{\left({}^{K_{wheel}}/_{R_m}\right)}{s+\left(\frac{K_{wheel}+K_v K_m}{R_m I_w}\right)} \tag{73}$$

The transfer function simplifies to a first order response. If K_{wheel} is chosen to be a value much larger than $K_v \cdot K_m$, then the wheel gain dominates and the entire wheel can be characterized as a simple first order equation [13]. This is indeed what was seen in the Bode plot of Fig. 17. For a high K_{wheel}, the system has a constant roll-off, infinite gain margin, and a phase margin of 90°. Considering the values for K_{wheel}, K_v, and K_m, it can be seen that the wheel gain of 600 is considerably larger than the product of K_v and K_m, 8.9e-7. Over short time periods, as suggested by the Bode plot, the wheel should act approximately like a first order system that delays the request for torque by some small time constant.

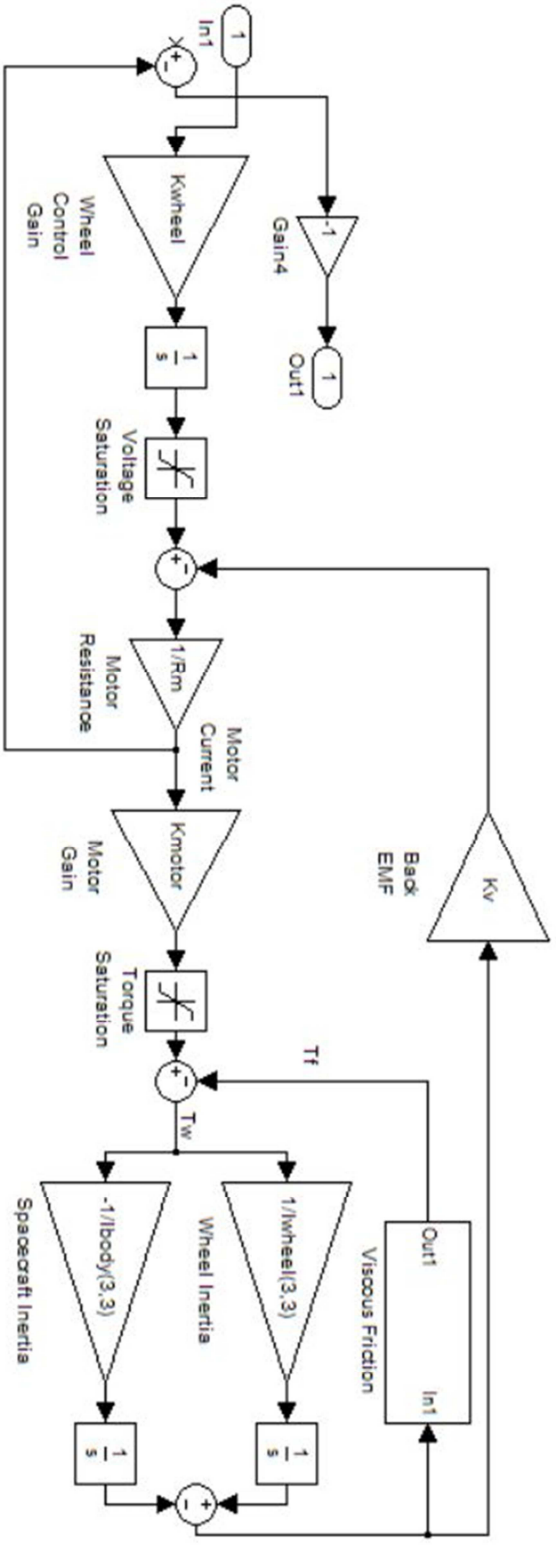

Fig. 16 Reaction wheel block diagram set up for frequency response analysis.

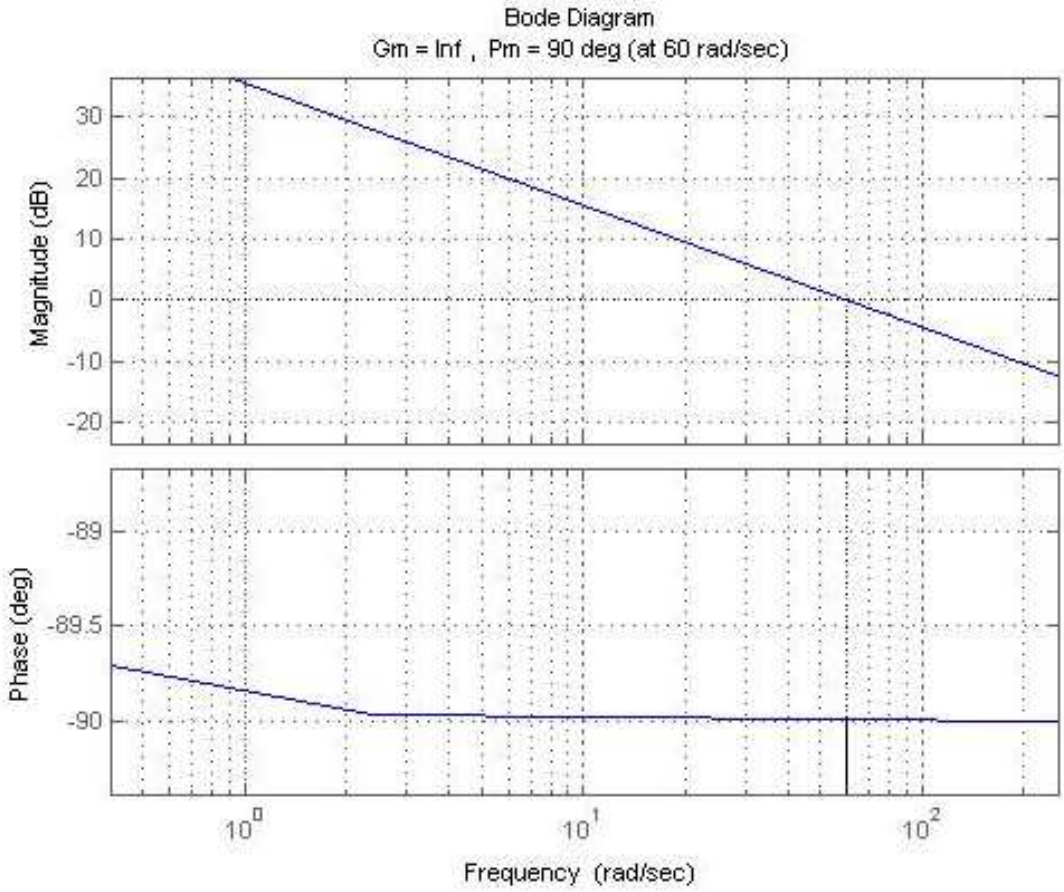

Fig. 17 Bode plot of the reaction wheel unit. The reaction wheel is stable and will have a relatively high bandwidth.

C. Analysis of Magnetorquer

The magnetorquer is a simple control system that is used purely to remove torque from the system. No sensors have been implemented into the analysis of this design and actual knowledge of the magnetic field may be poor. It is not important to resolve the magnetic field to any high degree because this system is meant only for the purposes of removing torque, not for maintaining a high accuracy of pointing. As seen in Fig. 18, the magnetorquer block, is activated by a relay that receives the absolute value of the momentum in the system and compares it to saturation limits. Because it is good practice

to add margin to theoretical limits, the magnetorquer should be active well before the actual maximum saturation. Activation at lower saturation levels requires the de-torqueing maneuvers to be more frequent, but desirably lowers amount of momentum being dumped. The reason to set a saturation limit of 50% maximum saturation is threefold: 1) it lowers the spin speed that the motor must maintain, 2) the motor takes less power, and 3) it requires a lower magnetic moment to be produced from the magnetorquers when de-torqueing. Because it is also desirable to avoid operating the wheel near the region where coulomb friction dominates the friction forces, a minimum desired amount of 10 rpm has been chosen.

Because utilizing the magnetorquer to exert authority over the pointing angle relies on the accuracy of the magnetic model, it is desirable to have the magnetorquer active only when necessary. Rather than allow the magnetorquers to be on at all times, a relay was designed to deactivate the momentum maneuver when the wheel speed drops to 10 rpm. Actively choosing to turn off the magnetorquer limits the opportunity for the magnetorquer to interfere with the reaction wheel's operation.

To choose a proper K_{mag} gain, a few simulations were performed. The performance gain must be compared to wheel response time, dump maneuver duration and magnetic moment performance. Too much gain would create more torque than could be compensated by the wheels and would require oversized magnetorquers, while too little gain would cause the system to never effectively overcome the secular disturbances. It is also important to be aware of the limits, or magnetic saturation, of the magnetorquer, as will be discussed in later sections.

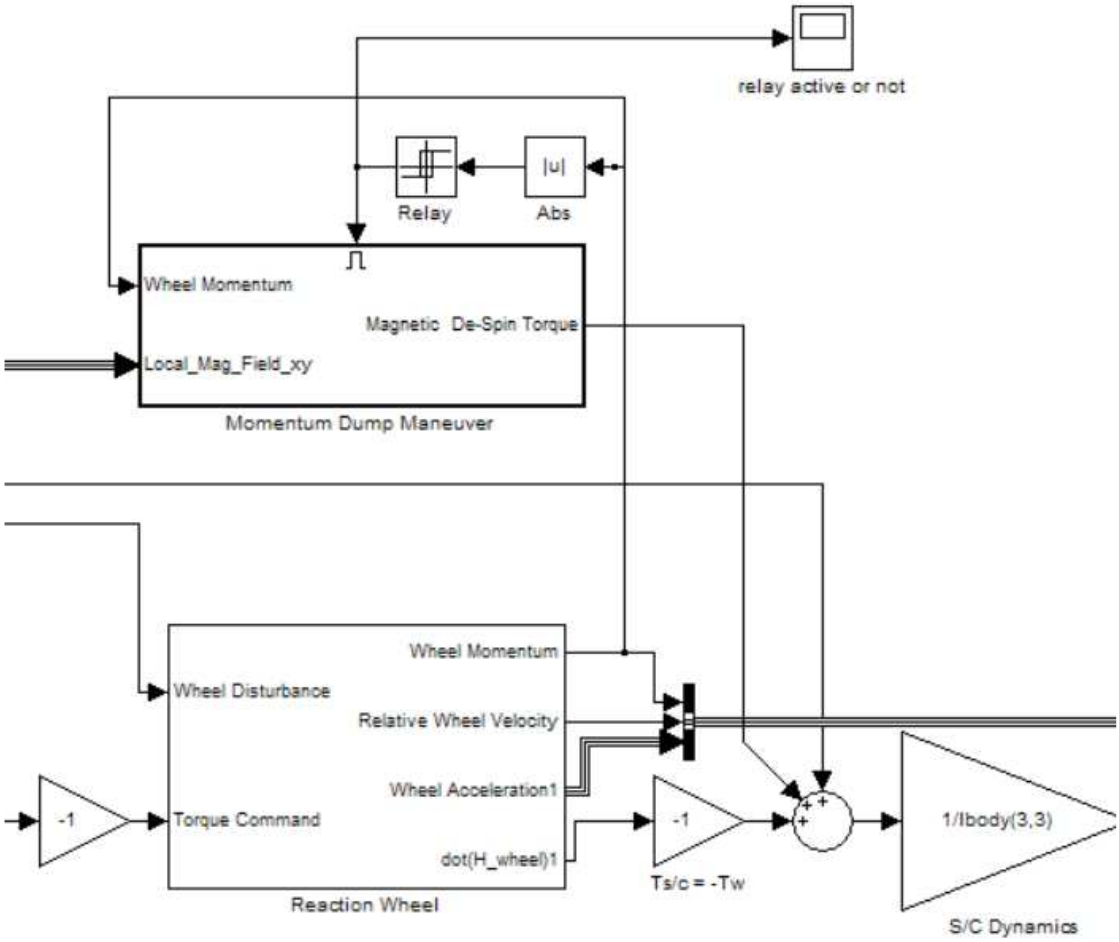

Fig. 18 Momentum change maneuver block implemented into simulation.

A K_{mag} of 8e-4 was found to desaturate the wheels in about 1.5 hours. The wheels typically reach 50% saturation in 6.25 hours; therefore, the spacecraft will typically spend 20% of its operational time de-torqueing. During the momentum dumping maneuver, the rapid initial desaturation command degrades pointing precision from about ± 0.01° to ± 0.07°.

Currently, several manufacturers are producing magnetorquers for CubeSats for commercial sale. Clyde Space, SSBV, and NSS all sell magnetorquers for CubeSats that

operate in the range of 0.2 $A \cdot m^2$ and have the attractive quality of operating at 5 V and 200 mW. Because of the ready availability of 0.2 $A \cdot m^2$ magnetorquers, it is assumed that a magnetorquer of similar performance can be manufactured for this CubeSat.

D. Analysis of Friction Compensator

It is important to note that a model is only as good as its approximation of real life phenomena. In this design, the measurement of the wheel's state is assumed to be known perfectly. This is impossible of course, so some error will exist in the ability to precisely determine the magnitude of the friction losses. Additionally, and perhaps more importantly, without actual hardware, the friction loss in the wheel is assumed to be some idealized viscous friction. In truth, the viscous friction will be some nonlinear function based on any number of factors, such as degradation, temperature, speed, pressure, etc.[†††] Here, the simulated friction acting on the wheel in this model is precisely matched and fed back into the system's control. Friction is not directly measureable and little discrepancies between an actual reaction wheel and model could have error-inducing effects. Therefore, extensive testing must be performed to match the compensator as accurately as possible to the friction that will be experienced in flight.

The compensated reaction wheel was run through an open loop response test to find the effect of the new compensator on its stability. Figure 19 shows the bode plot of the combined wheel and compensator loop. Without adding any poles to the system, the stability remains largely unchanged. The system maintains its natural frequency, phase

[†††] Not to mention the fact that this thesis does not utilize one of the more complicated models of friction.

margin and infinite gain margin. This shows that the system was not suddenly driven unstable with the addition of the dynamic compensator.

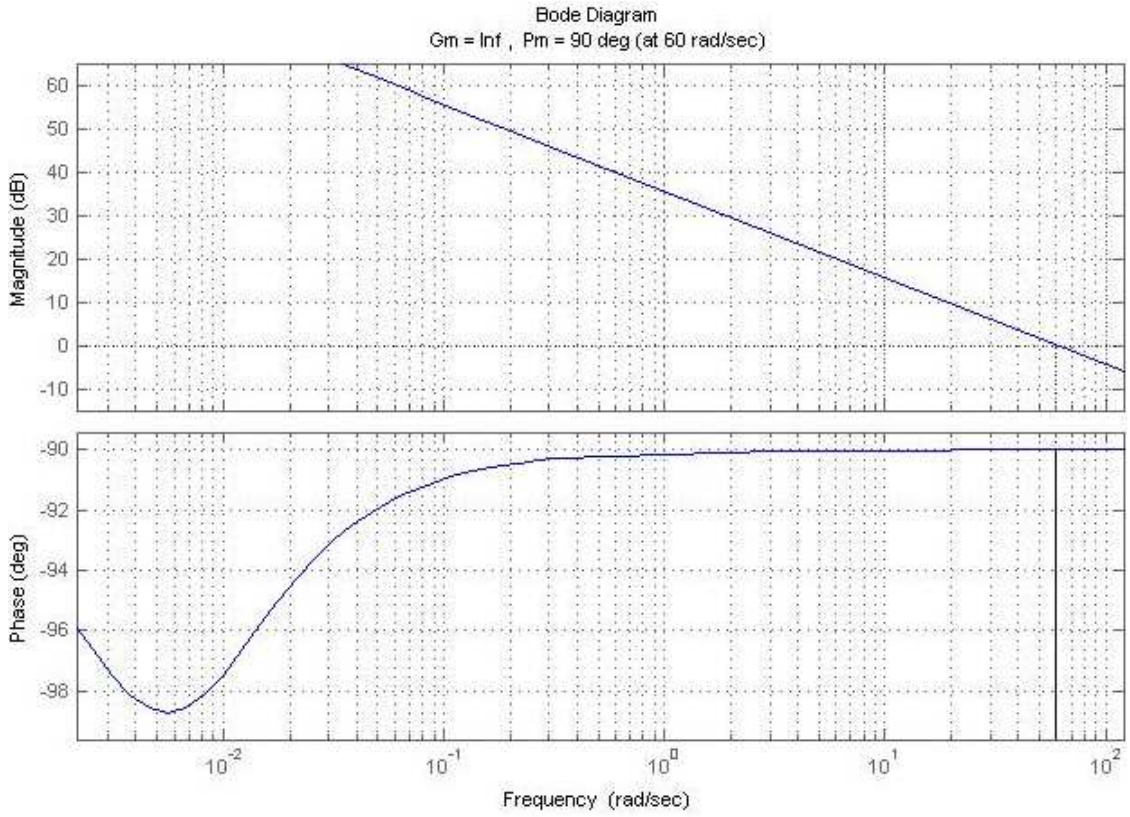

Fig. 19 Stable wheel response with added friction compensator.

Effectiveness of the concept of a friction compensator can be seen when comparing the position of the spacecraft over time when utilizing or abstaining from using a friction compensator. Figure 20 compares position over the course of 9 hours when the spacecraft is subjected to disturbance torques with and without compensation. The spacecraft is commanded to hold position with its x positive face nadir, at spin angle 0^o. Over 9 hours, the uncompensated simulation is seen to drift by approximately 0.25^o over 5.5 hours.

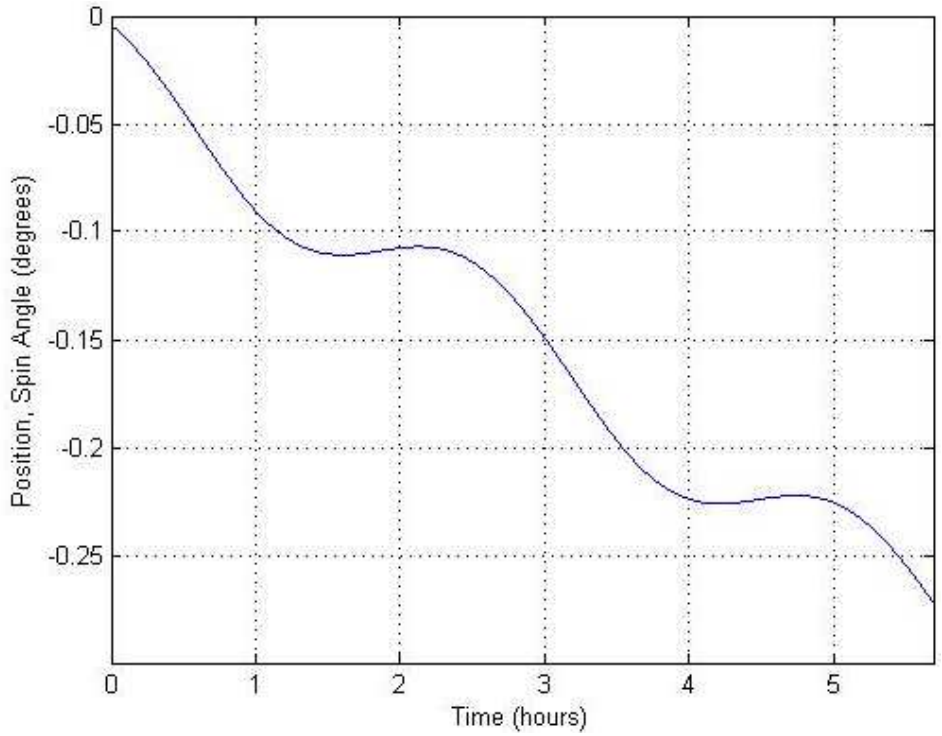

(a)

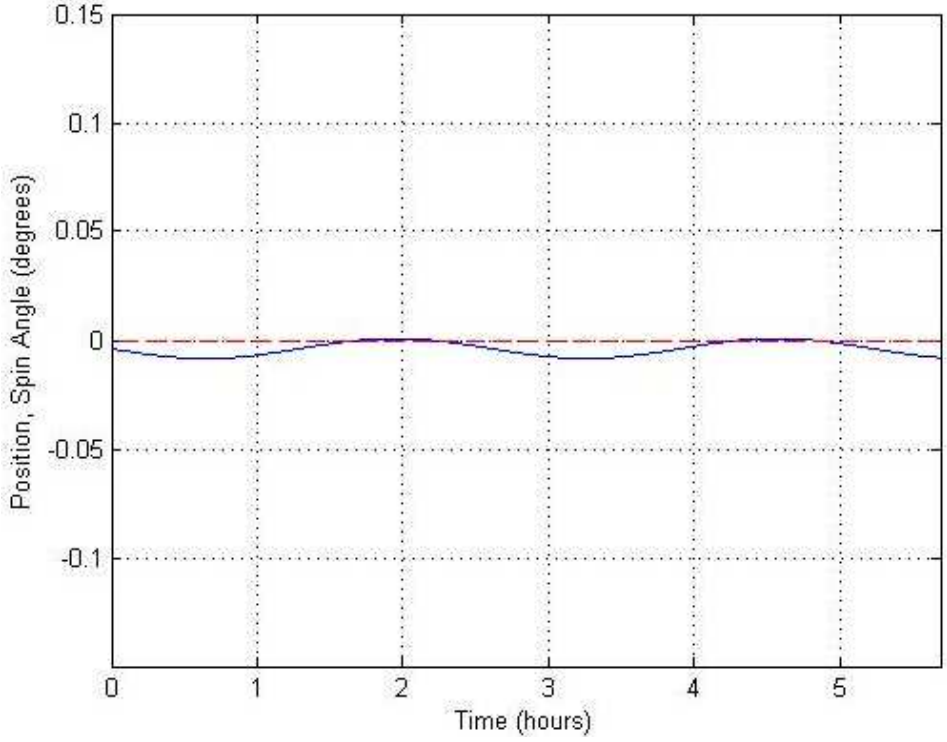

(b)

Fig. 20 Satellite friction compensator effectiveness. Spacecraft position (a) without and (b) with a friction compensator. Uncompensated satellite seen to diverge substantially.

E. Solver Properties

It must be noted that the proper choice of simulation solver is critical to resolve characteristics of the system. The Simulink program can utilize a number of different solvers to simulate a test. Table 3 compares the responses of the wheel torque when simulated with three different solvers. All variables are kept constant between simulations, but various solutions are obtained, showing that the numerical accuracy is dependent on which solver is chosen. While the ODE 45 and ODE23 solvers chatter with some steady state error, the stiff ODE 15s solver shows that the entire system is able to reach a convergence point sufficient to allow for precise system response. The steady state error in Table 3 is a measure of how well the wheel is able to meet its performance demands. That this error is influenced by solver method shows that it is important to choose a sufficiently accurate solution method. Because the torque values developed by the wheel are so small, the entire system can be diverged by a simple constant offset of an oscillating numerical inaccuracy. ODE 15s has been chosen as the solution method for all simulations because of its ability to converge the steady state oscillations.

Table 5 Solver accuracy chart. Torque response to a command for step input in simulation of Fig. 10. Input step height taken as one-half saturation torque. Oscillation due to numerical errors.

Solver	**Target Step Value [mN·m]**	**Steady State Oscillation Height [mN·m]**	**Steady State Error [N·m]**	**Settling Time [sec]**
ODE45 (Dormand-Prince)	0.2241	0.2205 to 0.22384	~1e-7	1.2
ODE23 (Bogacki-Shampine)	0.2241	0.22385 to 0.22433	~2e-8	1.1
ODE 15s (stiff/NDF)	0.2241	0.000	2.55e-8	1.6

F. Fully Integrated System Performance

To verify the entire system is stable when reaction wheel, compensator, disturbances and momentum dumping maneuvers are integrated, time response and frequency response trials have been performed. The momentum dumping maneuver operates in discrete time intervals and changes the equations of motion, so the stability must be tested with and without the de-torqueing maneuver being active. In the control law section, three sets of control laws were developed; for analysis, the control law gains have been set to the low performance gain mode, k_{frame} = 0.0052 and $k_{d,frame}$ = 0.0126.

The frequency response of the overall sub-system was analyzed for stability. To do so, the closed-loop was broken at the same location as it was for the control law analysis. The resulting Bode plots can be seen in Fig. 21. for both of the hold position and momentum dump maneuvers.

Perhaps surprisingly, the momentum dumping maneuver does greatly not affect the system stability. The overall system has a natural frequency of 3.83 rad/s and a corresponding bandwidth of 0.51 rad/s, 0.08 Hz. Nominally the system has a considerable 43.2 dB of gain margin and 67.7^{o} of phase margin. When the system performs a de-torqueing maneuver, this phase margin drops slightly to 67.5^{o}. It is commonly understood that systems should maintain gain margins of 6 dB and phase margins of 45^{o}. This indicates the system is sufficiently stable and has satisfactory margins which can tolerate the losses associated with incorporating the dynamics of mechanical systems.

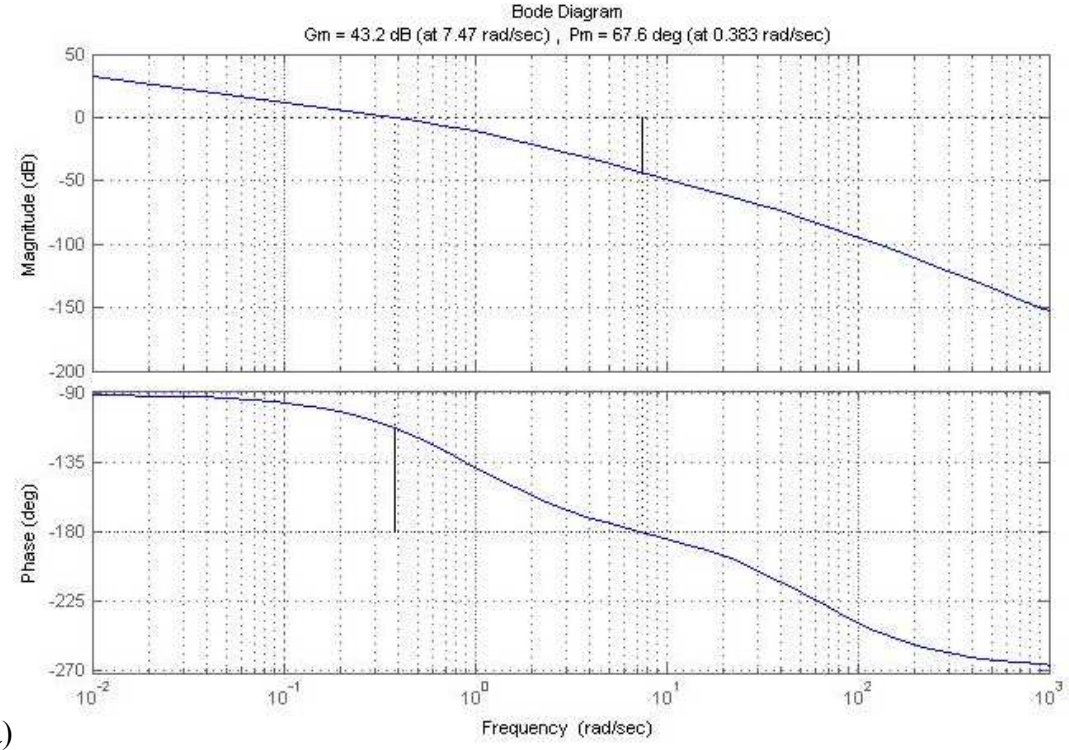

(a)

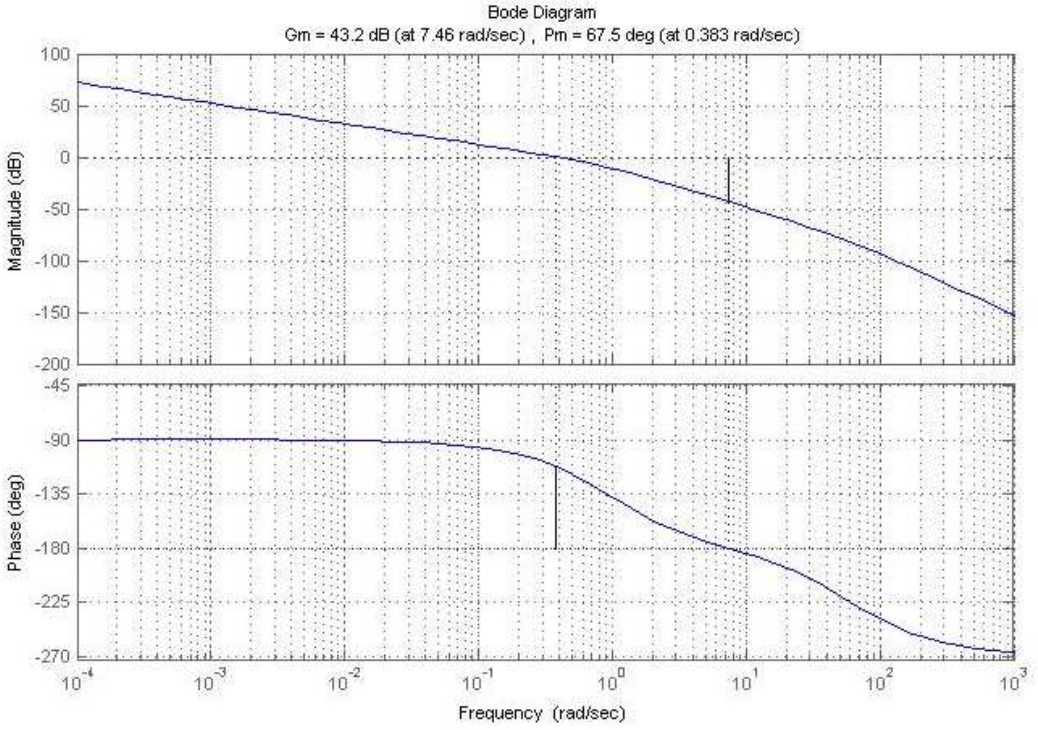

(b)

Fig. 21 The nearly identical frequency response of the fully integrated system during both of its maneuvers. Nominal flight under (a) hold-position command and (b) de-torqueing maneuver.

1. Station Keeping Simulation

The spacecraft must be able to maintain pointing control indefinitely. A simulation over the course of two desaturation maneuvers was performed and analyzed. The position with respect to time was plotted in Fig. 22. The satellite attitude can be seen to track the reference position with some offset and a slight, constant oscillation. The system has a steady state error of -13.7 arc sec and oscillates by ± 16.7 arc sec with a frequency of 0.7 mHz (one cycle every 2.63 hours).

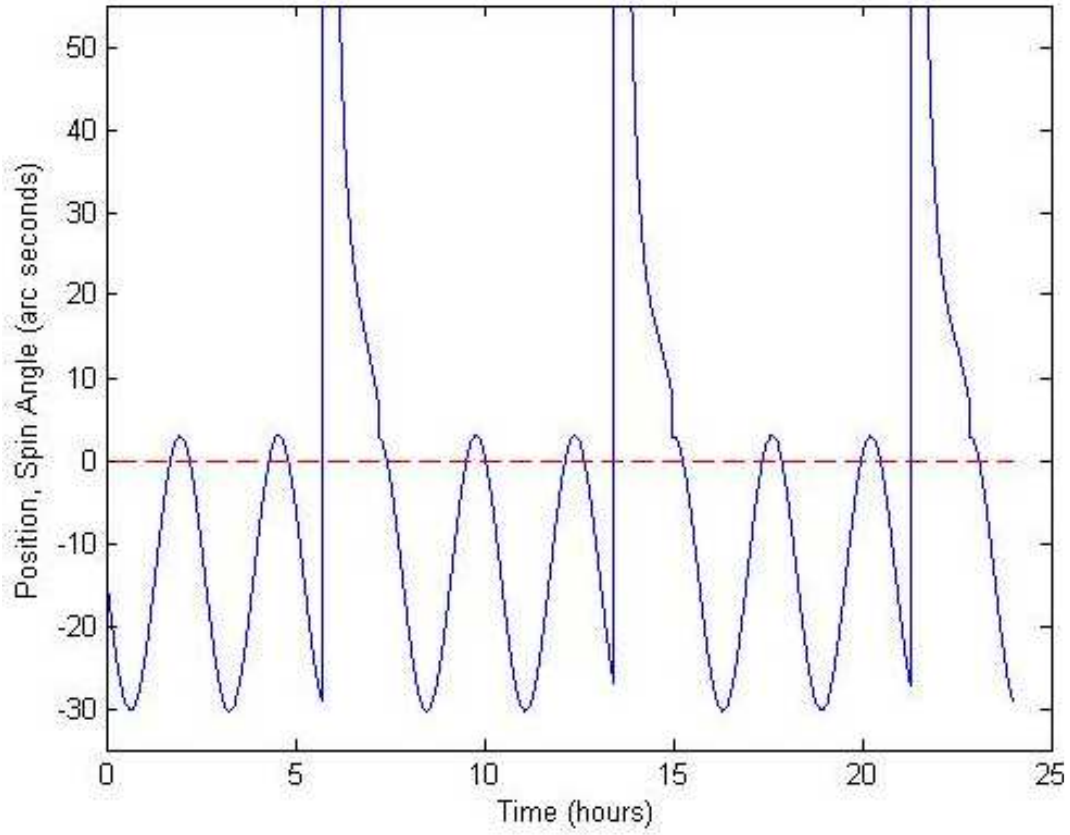

Fig. 22 Satellite pointing performance over 24 hours. Position of the satellite (solid line) as a response to the command to hold position (dotted line). Spacecraft pointing accuracy drops to 4.2 arc minutes during magnetorquer operation.

When the magnetorquer is engaged, the position error spikes up to an offset of 4.22 arc minutes and quickly improves as relatively large magnetic torque brings the excess momentum to a minimum. The system is able to maintain control over several orbits and can be expected to maintain its authority if the simulation was extrapolated out to a much greater extent. Wheel acceleration was inspected and found to be well within limits. The maximum wheel torque deliverable by the system is 0.048 mN·m and requires 7.50e-6 N·m during the de-torqueing maneuver, 1.6% of its maximum torque. The limiting performance factor in the de-torqueing maneuver is the maximum magnetic moment that the magnetorquer can create. Maximum moment required from the magnetorquer is just under the saturation limit of 0.2 Amp·m^2.

2. Reaction Wheel Noise Response Simulation

Pointing accuracy is also sensitive to wheel noise. Accuracy is seen to drop when the wheel is subjected to a disturbance. This was modeled as a Gaussian distribution of white noise with a magnitude of 1e-6 N·m and a sample time of 0.1. The steady state error remains -13.7 arc seconds with the same cyclical profile as the simulation without wheel noise, which can be seen in Fig. 23. The pointing accuracy, however, drops to ±15.0 arc seconds, shown in Fig. 24. During the de-torqueing maneuver, the pointing accuracy closely matches the simulation without wheel noise. Without the ability to predict the stochastic noise being injected to the system, the best that the reaction wheel can hope to accomplish is to compensate for the noise. This delay causes the spacecraft to drift from the nominal orientation before it can be corrected. Because of this chatter, accuracy is lost.

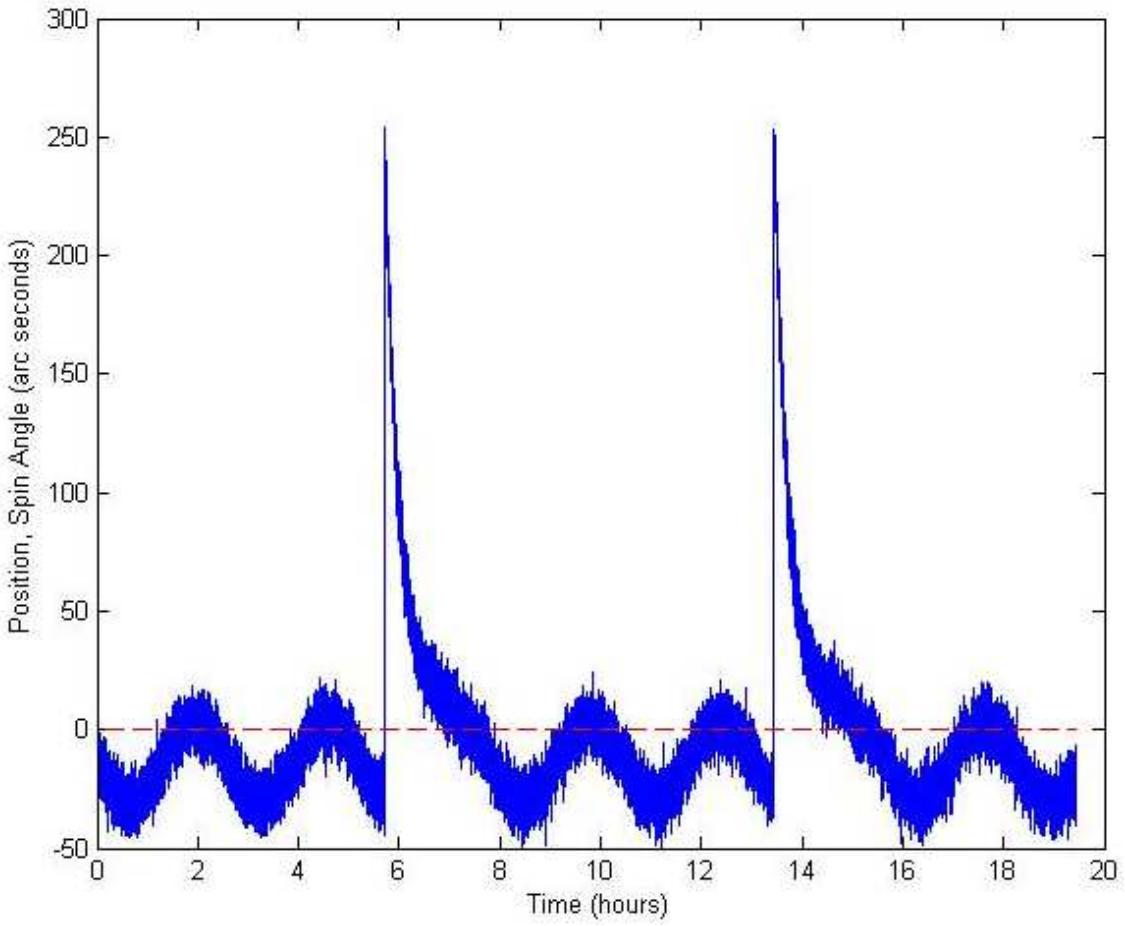

Fig. 23 Spacecraft position with reaction wheel disturbances. Response looks largely similar to the noiseless simulation but with degraded pointing accuracy.

3. Initiation Simulation

Another maneuver to consider is during the period of time when the spacecraft must stabilize itself after deployment. The design parameter is for the spacecraft to halt a rotation of 1 rpm, point the "x" positive face nadir, and dump accumulated momentum. This requirement is based off the notion that after deployment, or fault recovery, the spacecraft is expected to have some non-zero spin rate that needs to be suppressed. The worst case expectation is that the spacecraft is oriented such that it 180^{o} out of alignment and that it is rotating at 1 rpm.

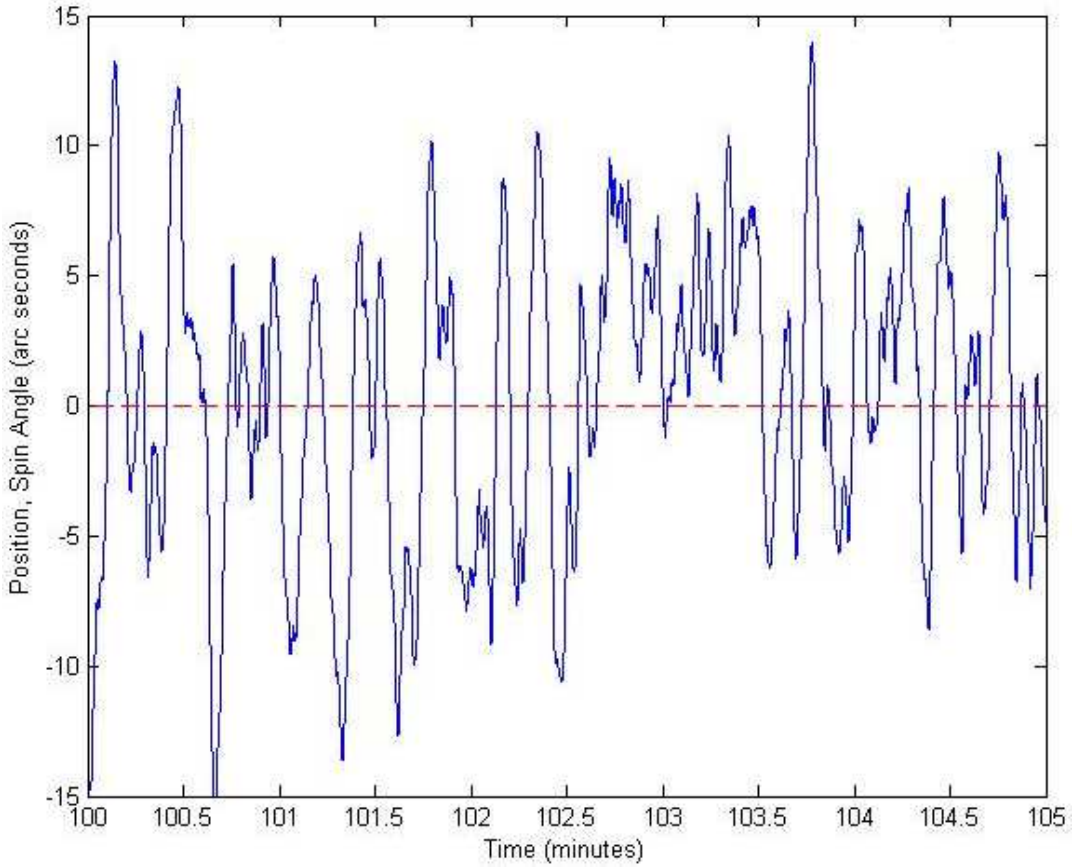

Fig. 24 Close view of spacecraft position noise with reaction wheel disturbances. Wheel motor noise on the order of micro Newton-meters causes considerable loss of pointing accuracy.

An intelligence should be built into the implemented control laws such that the system should utilize its initial velocity and position to travel the shortest distance to nominal alignment. This simulation does not relate 360^{o} to 0^{o}. If, for example, the spacecraft found itself at 270^{o}, it would travel 270^{o} in the reverse direction to 0^{o} – rather than traveling 90^{o} up to 360^{o} (which is physically the same as 0^{o}). Results of the initialization maneuver can be seen in Fig. 25. The initial condition of a positive velocity and orientation was manually set so that the spacecraft approaches nominal orientation in the direction of its velocity, in other words, the initial condition is set to a positive velocity of

1 rotation per minute and oriented to point toward -180º. If the position was set to +180º, the spacecraft would have to first kills its rotational momentum and then travel an unnecessary rotational distance to come back to 0º.

Crucially, the momentum capacity of the reaction wheel is sufficient to perform the entire initiation maneuver without tripping the magnetic de-torque maneuver. Figure 25 also shows the torque generation demands on the reaction wheel.

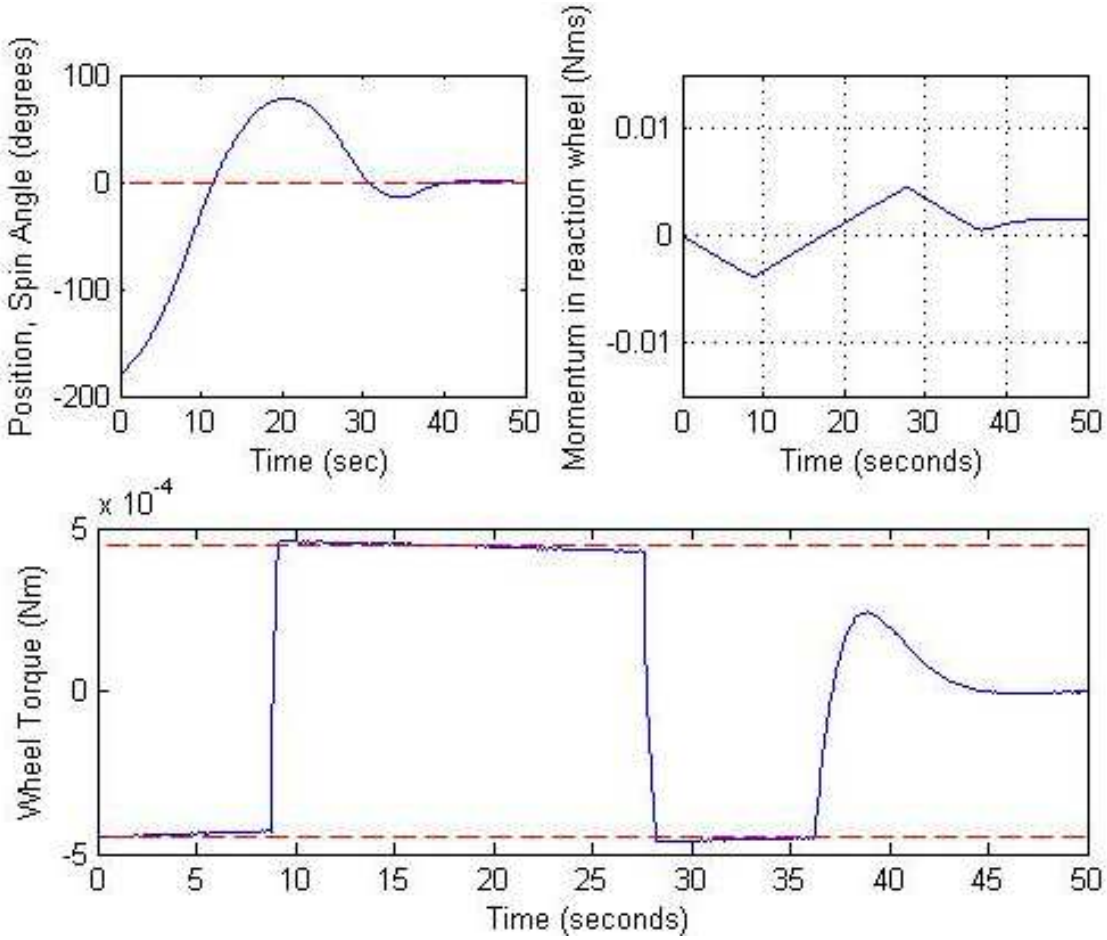

Fig. 25 Spacecraft performance during worst case initiation. Upper left view is the spin angle, upper right is momentum in the wheel, y-axis upper and lower limits are set to momentum saturation. Lower plot shows wheel torque saturating as controller quickly tries to reduce position to 0º. The motor becomes torque saturated if commanded to produce more torque than it is capable of; this is indicated by the red dotted line. Controller reaches nominal operation in 60 sec.

The motor is not sufficiently sized to provide the torque demanded by the control law is saturated for most of the maneuver. Eventually the system is able to stabilize, but wheel response will act nonlinearly and will take longer than anticipated by the control law. This is not an issue for this CubeSat because the maneuver duration is relatively short and extremely fast stabilization is not a critical aspect of the CubeSat mission. Though motor saturation carries risk of motor degradation, it is expected to happen only during initiation and is only a slight risk to mission health. To avoid the wear on the motor and the regions of nonlinear operation, a new flight maneuver could be developed to more gently lower the rotation rate from 1 rotation per minute to null. As it stands, the spacecraft is able to come to a nominal attitude in 60 sec. Wheel noise was not considered in this simulation.

4. Roll Command Simulation

As part of its daily operations, the spacecraft may be commanded to rotate to a given spin angle. Reasons for this might be to angle the antenna or point the camera at a specific target on Earth. Through simulations, it was found that the spacecraft can safely be commanded to rotate up to 6^{o} per sec, rotating 180^{o} in only 30 sec. to completely rotate 180^{o}, roughly 1% of the overall momentum capacity is transferred to or from the wheel. During this maneuver, the wheel accelerates at 88.6% of maximum acceleration, as seen in Fig. 26. This does not overly tax the system and can be done at will to reach whatever orientation is desired.

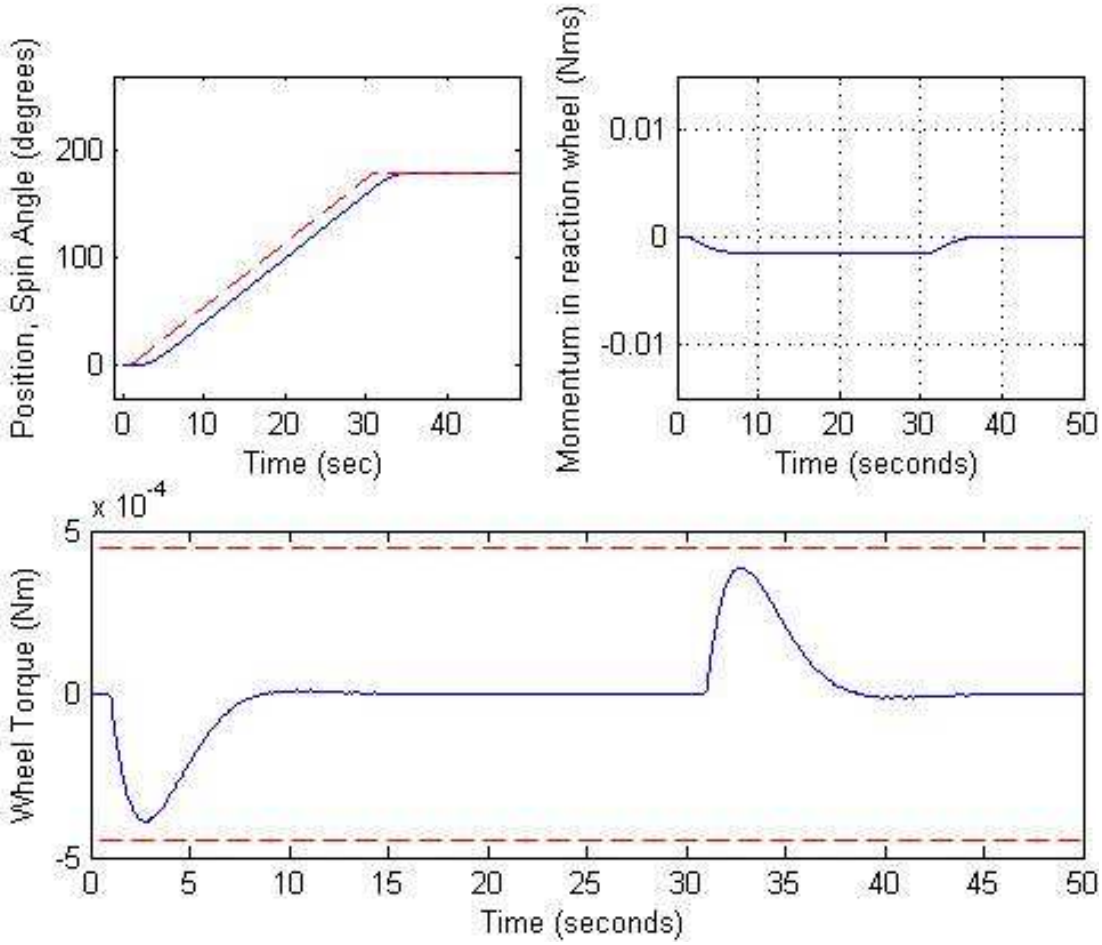

Fig. 26 Spacecraft performance to roll command at 6° per sec. Snapshot of the maneuver to rotate 180°, completed in roughly 40 seconds. Reaction wheel nears, but does not reach, torque saturation limits.

5. Summary of Simulation Results

The simulations performed on this model are an attempt to capture all the foreseeable scenarios in which the TechEdSat may find itself. These results show that the satellite is able to meet the requirements developed at the onset of this investigation. To recap, the satellite must suitably maintain attitude, actively control its nadir pointing angle with 1° accuracy, be designed to fit within 0.5U cube, and follow limits imposed by the power system.

Each simulation is shown to be able to meet mission objectives. During initiation, the spacecraft will become fully stabilized in under 1 minute and will be able to complete the maneuver without performing a momentum desaturation maneuver. In nominal operation, the spacecraft will reject disturbances and maintain attitude with less than 1 arc minute of accuracy for 80% of its saturation cycle (this includes the assumption of wheel noise). When utilizing magnetorquers to dump momentum, that accuracy error rises to less than 5 arc minutes, well below the 1^{o} accuracy requirements. If a new orientation of the spacecraft body frame is desired, the control system can roll the spacecraft at a rate of 6^{o}/sec and hold any orientation desired. Table 6 collects this information into a useful reference chart.

Table 6 Simulation results and spacecraft performance.

Maneuver	**Accuracy**	**Duration**	**Peak Wheel Torque [mN·m]**	**Peak Momentum [mN·m·s]**	**Notes**
Initiation	N/A	50 [sec]	0.482 (100% cap.)	4.48 (30% cap.)	Wheel torque saturation reached
Nominal hold	30 [arc sec]	6.26 [hours] 80%	0.004 (>1% cap.)	7.5 (50% cap.)	Limited by reaction wheel noise response
De-torque	4.22 [arc min]	1.47 [hours] 20%	0.011 (2% cap.)	7.5 (50% cap.)	Duration driven by magnetorquer performance
Roll	6 [deg/sec]	< 40 [sec]	0.387 (80% cap.)	1.43 (10% cap.)	Rate is wheel torque limited

X. Conclusion

A. System Review

This one-axis system has been designed to meet requirements set out in the system design parameters and is able to reject disturbances expected at its nominal orbital height. Certain assumptions have been made to complete the model. Chief among them is the assumption the no sensor noise affects the model, that the rotation rate in the yaw and pitch axes are small enough to not affect the dynamics, and that the exo-brake will not noticeably affect the inertia of the model. It is also assumed that the relatively strong magnetic field operates on a very weakly magnetic spacecraft to create the dominant environmental disturbance.

In all operations that the CubeSat is expected to perform, its reaction wheel has been determined to be sufficiently sized to meet design needs. The wheel is able to hold position with an accuracy much higher than the required 1^{o} during all operations. The system also has considerable gain and phase margins to verify its robust authority. The overall margins on the system requirements lead to confidence that an actual prototype will be able to meet the design requirements if built.

B. Future Work

Future work on this project could be performed to increase the accuracy of the model simulated. Because of the assumptions that serve to limit the design to a single axis, interplay of magnetorquer and exo-brake is lost. A three axis model that considers the interaction between the moments on the axes controlled by the exo-brake and the reaction wheel would be an interesting investigation. The current satellite is assumed to be a solid block of aluminum. If actual inertial values for the TechEdSat with exo-brake deployed could be found, the model's response characteristics may become more valid. The

assumption of perfect state information is also one that could also be improved upon. Realistic motor characteristics have been developed for the reaction wheel; these are, however, only approximations. Testing of actual hardware would bring the development out of the academic realm and into a realizable system. Developing the characteristics of sensor hardware-noise and accuracy and insert them into the simulations would more accurately capture satellite response and the possible levels of precision. This is expected to be the biggest improvement to model fidelity.

C. Lessons Learned

Unlike typical ADCS reaction wheels that have high power and small wheel inertia, this CubeSat study considers the exact opposite. Performance is largely limited by how little torque can be developed by a 5V motor. Interestingly, because the wheel's inertia can be compared to the satellite inertia, the relative momentum capacity of the wheel is tremendous (small changes in wheel spin speed will have a comparatively large effect on the satellite). In designing future reaction wheel systems, it may be useful to consider the ratio of wheel-to-body inertia. This design had an inertia ratio of 4.35e-3. This is considerably larger than the inertia ratio in [12], which had a ratio of 2.6e-7.

Disturbance torques are unforgiving on CubeSats. Although the resulting disturbance forces are small, the miniscule inertia of a CubeSat means that the space environment creates large changes in large wheel momentum capacity. This is an especially poignant fact in LEO, where the disturbances tend to be much larger than GEO. The CubeSat needs its momentum dumped much more frequently than initially anticipated because of this tendency to soak momentum.

As technological progress drives the creation of smaller electronic components and as micro-motors become more efficient, the control of CubeSats will become more sophisticated. With more and more advanced proficiency of small satellite attitude control new mission will be enabled on a smaller and cheaper scale than ever before. It is an exciting time to develop small satellite technologies.

XI. References

[1]Deepak, R. A., and Twiggs, R. J., "Thinking Out of the Box: Space Science Beyond the CubeSat," *Journal of Small Satellites*, Vol. 1, No. 1, 2012, pp. 3-7.

[2]Greenland, S., and Clark, C., "CubeSat Platforms as an On-Orbit Technology Validation and Verification Vehicle," *ESA Small Satellites and Services Symposium*, ESA, Funchal, Madeira, Portugal, 2010.

[3]"Small Satellite Technology State of the Art," Mission Design Division Staff, Ames Research Center., Rept. NASA/TP-2014-216648/REV1, Moffet Field, CA, July 2014.

[4]Larson, W. J., and Wertz, J. R., *Space Mission Analysis and Design*, 3rd ed., Microcosm Press, El Segundo, CA, 1999.

[5]Curtis, Howard D., *Orbital Mechanics for Engineering Students,* 2nd ed. Elsevier. 2009, Oxford, UK.

[6]Pignatelli, D., Nugent, R., Munakata, R., and Lan, W., "P-POD Mk. III Rev. E User Guide," The CubeSat Program, Rept. CP-PPODUG-1.0-1, Cal Poly San Luis Obispo, CA, March. 2014.

[7]"NanoRacks CubeSat Deployer (NRCSD) Interface Control Document," NanoRacks, LLC, Rept. NR-SRD-029, Huston, TX, Dec. 2013.

[8]Lee, G. Y., et al., "Mechanical Considerations of Release and Spin-up of Constellation Microspacecraft," Science Closure and Enabling Technologies for Constellation Class Missions. UC Berkeley, California., 1998.

[9]Rossoni, P., Cooperrider, C., and Durback, G., "Deployment Mechanism for the Space Technology 5 Micro Satellite," 37th *Aerospace Mechanisms Symposium*, NASA 20040082383, Johnson Space Center, Huston, TX, May 2004.

[10]Bender, E., "An Analysis of Stabilizing 3U CubeSat Using Gravity Gradient Techniques and a Low Power Reaction Wheel." Senior Project, Department of Aerospace Engineering, Cal Poly San Luis Obispo. San Luis Obispo, CA. 2011.

[11]Curti, F., Romano, M., Bevilacqua, R. "Lyapunov-Based Thrusters' Selection for Spacecraft Control: Analysis and Experimentation." Journal of Guidance, Control, and Dynamics. Vol. 33, No. 4, July-Aug 2010. DOI: 10.2514/1.47296.

[12]Carrara, V., and Kuga, H. "Torque and Speed Control Loops of a Reaction Wheel," *11th International Conference on Vibrational Problems*, Department of Civil Engineering of Faculdade de Ciências e Tecnologia of Universidade Nova de Lisboa and Institute of

Mechanical Engineering of Instituto Superior Técnico of University of Lisbon, Lisbon, Portugal, Sept. 2013.

[13]Sidi, M. J., *Spacecraft Dynamics and Control*, 1st ed., the Press Syndicate of the University of Cambridge, New York, NY, 1997.

[14]Wang, P., Shtessel, Y. B., Wang, Y. "Satellite Attitude Control Using only Magnetorquers," System Theory, 1998. Proceedings of the Thirtieth Southeastern Symposium, pp.500,504, 8-10 Mar 1998 doi: 10.1109/SSST.1998.660124.

[15]Peters, E., et al, "Design and Functional Verification of a Mechanism for Dual-Spinning CubeSat," 42*nd Aerospace Mechanisms Symposium*, NASA, Goddard Space Flight Center, Greenbelt, MD, May 2014.

[16]Fadly, M., Sidek, O., and Azlin. "Development of Attitude Determination for Student Pico-Satellite INNOSAT" *Regional Conference on Mechanical and Aerospace Technology*, AUN/SEED-Net and Jica, Bali, Feb 2010.

[17]Turner, Andrew J. "An Open-Source, Extensible Spacecraft Simulation and Modeling Environment Framework." Masters Thesis, Department of Aerospace Engineering, Virginia Polytechnic Institute State University. Blacksburg, Virginia. 2003.

[18]"US/UK World Magnetic Model – Epoch 2015.0 Main Field Horizontal Intensity (H)," NOAA Geomagnetic Data & Information [online database], URL: http://www.ngdc.noaa.gov/geomag/WMM/data/WMM2015/WMMMaps2015.zip [cited 1 October 2015].

[19]Bate, R. R., Mueller, D. D., and White, J. E., *Fundamentals of Astrodynamics*, 1st ed., Dover Publications, Inc., New York, NY, 1971.

[20]Hastings, D. and Garrett, H., *Spacecraft Environment Interactions*, 1st ed., Cambridge University Press, New York, NY, 1996.

[21]Harris, M., and Lye, R., "Spacecraft Gravitational Torques," NASA SP-8024, 1969.

[22]Levine, W. S., *Control System Applications*, CRC Press LLC, Boca Raton, Florida, 2000.

[23]Carrara, V. and Kuga, H. K., "Estimating Friction Parameters in Reaction Wheels for Attitude Control," Mechanical Problems in Engineering, Vol. 2013. 2013. Hindawi Publishing Corporation. Article ID 249674.